

ALMA MATER STUDIORUM - UNIVERSITÀ DI BOLOGNA

SCUOLA DI INGEGNERIA E ARCHITETTURA

DIPARTIMENTO DI INGEGNERIA INDUSTRIALE - DIN

CORSO DI LAUREA MAGISTRALE IN INGEGNERIA MECCANICA

TESI DI LAUREA

in

Meccanica delle Macchine M

**DIRECT KINEMATICS
OF UNDERACTUATED CABLE-DRIVEN
PARALLEL ROBOTS:
SENSITIVITY TO REDUNDANT MEASUREMENTS**

CANDIDATO:
Sara Gabaldo

RELATORE:
Prof. Ing. Marco Carricato

CORRELATORI:
Edoardo Idà
Marco Troncossi

Anno accademico 2021/2022

Sessione 23/03/2022



This work is licensed under the Creative Common
Attribution-NonCommercial-ShareAlike 4.0 International (CC BY-NC-SA 4.0).

To view a copy of this license, visit
<https://creativecommons.org/licenses/by-nc-sa/4.0/legalcode>

Abstract

Underactuated cable-driven parallel robots (*UACDPRs*) shift a 6-degree-of-freedom end-effector (*EE*) with fewer than 6 cables. This thesis proposes a new automatic calibration technique that is applicable for under-actuated cable-driven parallel robots. The purpose of this work is to develop a method that uses free motion as an exciting trajectory for the acquisition of calibration data. The key point of this approach is to find a relationship between the unknown parameters to be calibrated (the lengths of the cables) and the parameters that could be measured by sensors (the swivel pulley angles measured by the encoders and roll-and-pitch angles measured by inclinometers on the platform). The equations involved are the geometrical-closure equations and the finite-difference velocity equations, solved using the least-squares algorithm. Simulations are performed on a parallel robot driven by 4 cables for validation. The final purpose of the calibration method is, still, the determination of the platform initial pose. As a consequence of underactuation, the *EE* is underconstrained and, for assigned cable lengths, the *EE* pose cannot be obtained by means of forward kinematics only. Hence, a direct-kinematics algorithm for a 4-cable *UACDPR* using redundant sensor measurements is proposed. The proposed method measures two orientation parameters of the *EE* besides cable lengths, in order to determine the other four pose variables, namely 3 position coordinates and one additional orientation parameter. Then, we study the performance of the direct-kinematics algorithm through the computation of the sensitivity of the direct-kinematics solution to measurement errors. Furthermore, position and orientation error upper limits are computed for bounded cable lengths errors resulting from the calibration procedure, and roll and pitch angles errors which are due to inclinometer inaccuracies.

Contents

Abstract	5
1 Introduction	9
1.1 Topology of Cable Robots	9
1.2 Applications and Accuracy	10
1.3 Under-Actuated Cable Robots	12
1.3.1 Thesis goals and Outline	13
2 Modelling	15
2.1 Geometric Modelling	15
2.1.1 Definition of the fundamental geometric entities	15
2.1.2 First geometrical constraint on cables direction and computation of the swivel angle	17
2.1.3 Second geometrical constraint on cables direction and computa- tion of the tangency angle	17
2.1.4 Geometrical constraint on cables length	18
2.1.5 <i>UACDPR</i> characterization	18
2.2 First order Kinematics	19
2.2.1 Angular velocity and twist of the <i>EE</i>	19
2.2.2 Swivel angle time derivative	19
2.2.3 Tangency angle time derivative	20
2.2.4 Cable length time derivative	20
2.2.5 Jacobian matrices	21
2.3 Second order Kinematics	21
2.3.1 Angular acceleration and twist time derivative of the <i>EE</i>	21
2.3.2 Swivel angle second order time derivative	22
2.3.3 Tangency angle second order time derivative	22
2.3.4 Cable-length second order time derivative	23
2.4 <i>EE</i> free and controlled kinematics	24
2.4.1 Controlled and free pose-coordinates	24
2.4.2 Free twist and free pose-coordinates derivative	24
3 Initial Pose Estimation Problem	27
3.1 Initial Pose Estimation Problem with Incremental Encoders	28
3.1.1 Modelling	28
3.1.2 Simulation Results	29
3.2 Initial Pose Estimation Problem with Absolute Encoders	36
3.2.1 Modelling	36
3.2.2 Simulation Results	37

3.3	Initial Pose Estimation Problem with Incremental Encoders and Inclinometers on the Platform	40
3.3.1	Modelling	40
3.3.2	Simulation Results	42
4	Sensitivity indices	47
4.1	Kinematic Sensitivity Indices for <i>UACDPRs</i>	48
4.1.1	Sensitivities to errors on measured geometric variables	49
4.1.2	Sensitivities to Errors on Roll and Pitch Measurements	50
4.1.3	Maximum combined point-displacement and yaw errors	51
4.2	Sensitivity to Errors in Cable Lengths and Pitch and Roll Angles	52
4.2.1	Sensitivity Indices	52
4.2.2	Simulation Results	53
4.3	Sensitivity to Errors in Swivel Angles and Pitch and Roll Angles	57
4.3.1	Sensitivity Indices	57
5	Conclusions	59
5.1	Main Results	59
5.2	Open Issues	59
	Appendices	61
A	Backward finite difference method	63

Chapter 1

Introduction

Producing a defined motion is one of the basic tasks of a machine. By definition, a robot is a universal machine that can generate a freely programmable motion. A variety of mechanisms are known that can generate different types of motion, which can be characterized by the degree of freedom of the motion, its dynamic properties such as velocity and acceleration, and its accuracy. The idea of using cables to transport loads is very old. Even in ancient times, cables were used to lift loads in construction and similar applications. To this day, cranes are widely used in construction and industrial production because they are versatile and cost-effective. When the load needs to be accurately placed or even assembled, human workers attach a few handy ropes to the load to pull it into position, suppress load sway, or counteract disturbances from the wind. Each rope attached to the platform restricts one degree of freedom, and in practice, it is common for a few workers to work together to pull a load into position. Having established that the coordinated movement of the additional ropes provides control over the movement of the load, it is only a small step to use motor winches for pulling. The second step is to use a computer to synchronize the movement of the winches and perform predefined movements with the winches to move the load in the desired manner. A computer-controlled crane is nothing more than a cable-controlled parallel robot. In the field of robotics and motion generators, the idea of a robot that is purely suspended and driven by cables was introduced in the 1980s. Since then, a number of researchers around the world have taken up this idea to create a new generation of robotic systems that exploit the outstanding potential of using cables to actuate a robot. Using cables to control a mobile platform in space offers a number of promising advantages, most notably the ultra-lightweight design of the robot. The available literature mostly deals with specific aspects such as kinematics, statics, dynamics, and control of cable robots. In [1] the state of the art in cable-driven parallel robots is presented and a consistent theory and a well-defined terminology are proposed.

1.1 Topology of Cable Robots

Based on topology, robots are classified into serial or parallel manipulators. Mechanical structures consisting of a sequence of joints and links, each joint being actuated, are called open kinematic chains. The resulting mechanism is called a serial robot. If instead more than one kinematic chain is connected to the end effector, the resulting mechanism is called a parallel robot. When the number of chains equals the number

of actuators, the robot is called fully parallel. A cable-driven parallel robot is a special type of parallel kinematic machine or parallel robot, and consists of a mobile platform, a fixed machine frame, and n cables attached at their distal end to the mobile platform and at their proximal end to the machine frame. The lengths of the cables are changed by an actuation system called winch. In most robots, the winches are permanently attached to the machine frame to facilitate electrical connection to the power and control system. Many cable robots use sensors to measure the effective length of the cables: for example, by encoders on the drum or with linear measuring systems on pulleys. Alternatively, the position and orientation of the mobile platform can be measured directly. For some applications, it is also necessary to determine the tension in the cables. This is usually done by force sensors connected to one end of the cable or to some pulleys in between. The size of the mobile platform can vary greatly: it can have a weight of a few grams and dimensions of a few millimeters; there are also examples of huge platforms, such as the collector of the Arecibo telescope (Fig. 1.1), which consists of a triangular platform of 9×10^5 kg suspended in the air 150 m above the base by means of 18 cables emanating from three reinforced towers, one of which is 110 m high and two 80 m high, with the top of the three towers at the same height. The most important properties for cable robots are the relative position of the distal anchor points with respect to the platform reference point, the center of gravity, the mass, and the inertia tensor. The machine frame is the mechanical structure that supports the winches and the proximal anchor points. In many laboratories and industrial configurations, the machine frame is a closed frame structure made of steel or aluminum bars. Especially for larger robots, the winches can also be attached to decentralized structures such as towers or buildings. It has also been proposed to use winches or cables on multiple flying or swimming structures such as helicopters [2], balloons, ships, and submarines. The cables can be made from a variety of materials. The most commonly used are steel and synthetic fibers such as high modulus polyethylene fibers.

1.2 Applications and Accuracy

Cable robots have been proposed for a very wide range of applications, such as production engineering, logistics, construction, motion simulation and entertainment. In Fig. 1.2 an example of a cable robot used to position TV broadcast cameras over a sports playing field is reported. As with many other robotic systems, the development of new ideas for applications usually involves replacing a predominantly manual or mechanized process with a robotic solution that enables fully automated operation. Cable robots can open up new application areas where industrial robots cannot be used due to limitations in terms of workspace size, payload or required cycle time. Cable robots also offer other advantages, such as minimal installation effort, easy transport and use, or improved quality.

The precision of a robotic system is determined by its accuracy and repeatability: these performance indices directly determine the robot's ability to properly perform its task. A robot's positional accuracy describes its ability to move its reference point to the desired absolute position in space, and is an important performance indicator for all types of robots. Repeatability is a measure of the deviation between the actual position reached by the end effector when approaching a desired position in space and the position reached in previous attempts to reach the same desired position. Repeatability is affected by the reproducibility of the motion in the actuators and in the mechanics.



Figure 1.1: Collector of the Arecibo Observatory. By H. Schweiker/WIYN and NOAO/AURA/NSF - <https://www.flickr.com/photos/nasablueshift/8288406364/>, CC BY 4.0, <https://commons.wikimedia.org/w/index.php?curid=113226349>

Effects such as elastic responses, control errors, and sensor errors affect the repeatability of the motion. Inaccurate cable length measurements caused by imperfect mechanics, control errors, and elastic deformation directly affect end effector accuracy. Elastic cables allow for greater elongation, however, positioning accuracy decreases as the stiffness of the cables decreases. For large-scale robots, one must also consider the elastic deformation of the robot frame. Consequently, accuracy decreases as the size of the robot increases. Therefore, the position measurement, control system, and all mechanical parts of the winch system must be designed so that the actuator's motion is precisely rendered to the cable length. Although considerable effort is made in the design, manufacture, and assembly of robots to build the robot exactly to design specifications, errors and uncertainties in the robot's geometry cannot be avoided. Therefore, improving accuracy through calibration is an important issue during robot commissioning. Calibration is the process of estimating the actual numerical values of the robot's geometric design parameters. Normally, it is assumed that the nominal parameters are given, where the nominal parameters are the ideal values established as a result of the design process. Thus, calibration is a particular way of identifying model parameters, where the model to be identified is a kinematic model and the parameters sought relate to the geometry of the robot.

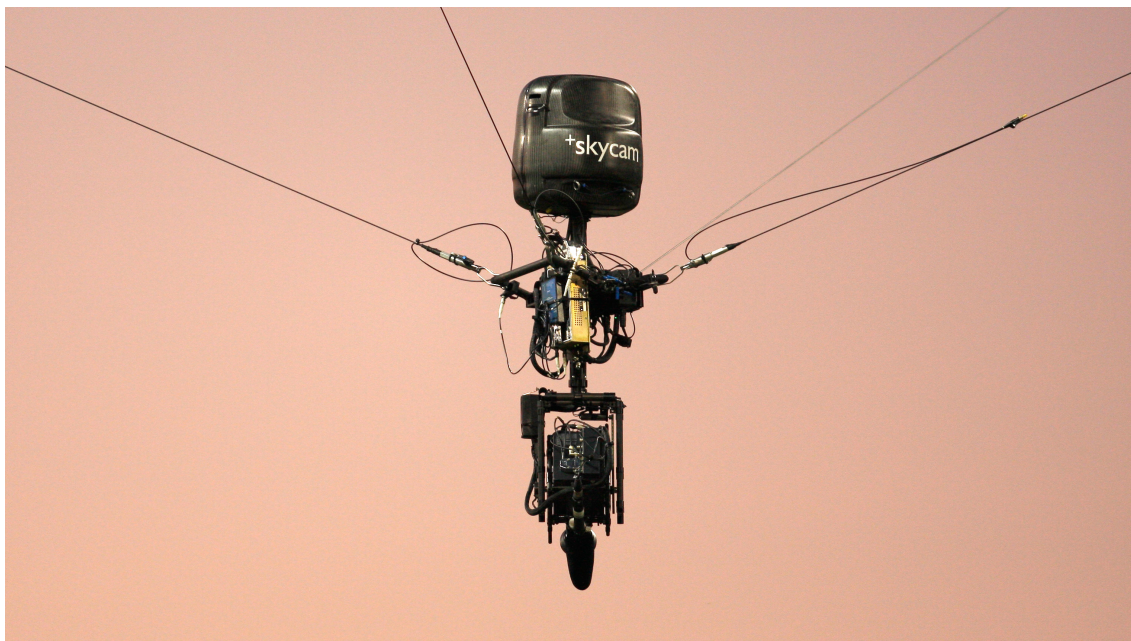


Figure 1.2: Cable robot used to position TV broadcast cameras, by Despeaux - Own work, CC BY-SA 3.0, <https://commons.wikimedia.org/w/index.php?curid=7852833>

1.3 Under-Actuated Cable Robots

The first cable robots classification that considers the number of cables and the controllable degrees-of-freedom of the mobile platform was introduced in [3]. If the number of cables is less than the number of degrees of freedom, the robot is classified as underconstrained. When the cable robot is underconstrained, a number of characteristics differ from the fully constrained case. Such robots are always operated in a suspended configuration, where the winches are located above the mobile platform, and gravity is additionally used to keep cables taut. Nevertheless, some degrees of freedom generally cannot be controlled by the cables. The number and direction of controllable degrees of freedom vary throughout the workspace.

As for any other underactuated manipulator, only n independent directions of motion can be generated by the actuators. When the number of cables n is less than six, there are $6 - n$ linearly independent directions in which no infinitesimal motion that is consistent with the constraints imposed by the cables can be generated. For such cable robots, new theoretical problems arise, such as the determination of the static equilibrium, that requires a different modeling approach than for the fully constrained cable robots. The determination of *UACDPRs* static equilibrium poses involves both geometric constraints as well as static equations. Different solutions to this problem have been proposed, for spatial robots with three [4], four [5], five [6] and, more generally, n [7] cables. A different problem arises when, assigned a certain law of motion to actuators, one wants to determine poses of the moving platform, for example, to be able to give feedback while the robot is moving. As mentioned, geometrical constraint equations are always underconstrained and, when one leaves the field of statics, the pose of the *EE* evolves according to *UACDPR* dynamics. The employment of dynamic equilibrium equations entails knowledge of inertial parameters, which may vary over time, and the integration of second-order differential equations, which is computa-

tionally heavy and difficult to perform in real-time. Alternatively, it is possible to solve forward kinematics by making use of extra-measures, as already proposed for classical parallel robots [8, 9], *CDPRs* [10, 11] and *UACDPRs* [12].

1.3.1 Thesis goals and Outline

This thesis focuses on a practical problem for *UACDPRs*, namely calibration. A major problem in the practical use of underactuated *CDPRs* is the estimation of the *EE* initial-pose. In fact, when the machine is turned on in a general starting condition, the *EE* pose is usually not known, but its knowledge is essential for any subsequent operation.

Chapter 2 is dedicated to the general kinematic modeling of *UACDPRs*. The geometric constraints imposed on the moving platform by cables and pulleys are analyzed, as well as their first and second-order time derivatives. The concepts of *EE free motion* and *controlled motion* are introduced and the basic rules for their description are presented.

Chapter 3 introduces an automatic calibration procedure for the estimation of the initial pose of a generic, suspended, underactuated *CDPR* that relies on data acquired during free motion of the *EE*. Three different algorithms are proposed:

- the first only relies on incremental measurements of swivel angles
- the second relies on absolute measurements of swivel angles
- the latter is based on incremental measurements of swivel angles and on measurements of roll and pitch orientation parameters performed by static inclinometers placed on the platform

Results of simulations are presented and discussed.

Chapter 4 aims to evaluate the sensitivity of position and yaw to errors in acquired measurements. The theoretical sensitivities of the direct-kinematics solution to measurement errors are defined, and these definitions are used to determine the maximum error of the direct kinematics solution when the errors in swivel angles, cable lengths, and pitch and roll angles are bounded within certain limits. Once a procedure is defined to determine how errors in the results obtained by the calibration algorithm affect the determination of the initial pose, the reliability of the results obtained in Chapter 3 can be evaluated.

Finally, in Chapter 5, conclusions are drawn and some remaining open questions are analyzed.

Chapter 2

Modelling

The purpose of this Chapter is to introduce the mathematical model of a generic 6-DoF n -cable *UACDPR*. The robot moves in the Special Euclidean space of dimension 3 ($SE(3)$) by means of cables modelled as straight line segments, massless and inextensible. Each cable is guided into the workspace by a swivel pulley, they are all coiled and uncoiled by servo-controlled winches, and their lengths are assumed to vary proportionally to actuator displacements.

2.1 Geometric Modelling

2.1.1 Definition of the fundamental geometric entities

An *UACDPR* in $SE(3)$ consists in a mobile platform coupled to the base by $n < 6$ cables. In order to describe the pose of the moving platform, $Oxyz$ (an inertial frame) and $Px'y'z'$ (a mobile frame attached to the platform) are considered. Moreover, a position vector \mathbf{p} of P , and a rotation matrix \mathbf{R} (Fig. 2.1) are defined. \mathbf{R} is parametrized by roll-pitch-yaw (*RPY*) angles $\boldsymbol{\epsilon} = [\phi, \theta, \psi]^T$ namely:

$$\mathbf{R} = \mathbf{R}_z(\psi)\mathbf{R}_y(\theta)\mathbf{R}_x(\phi) \quad (2.1)$$

where $\mathbf{R}_x(\cdot)$, $\mathbf{R}_y(\cdot)$ and $\mathbf{R}_z(\cdot)$ are elementary rotation matrices about x , y and z axes. *EE* generalized coordinates are finally denoted by $\boldsymbol{\zeta} = [\mathbf{p}^T \boldsymbol{\epsilon}^T]^T$.

Each pulley is mounted on a hinged support, and is free to rotate around a hinge axis z_i , also called swivel axis. The swivel axis is tangent to the pulley in point D_i , whose coordinates are constant in the inertial frame and whose position is denoted by the vector \mathbf{d}_i .

Each pulley drives a cable into the workspace: the cable enters the pulley's external groove in point D_i and exits from it at point B_i . The position of point B_i is (in general) variable in both fixed and inertial frame, and depends on the geometrical model [13,14] of the pulley (which is detailed hereafter).

Each cable is thus attached to the platform at point A_i , whose coordinates are constant in the mobile frame and whose position is denoted by the vector ${}^P\mathbf{a}'_i$. The coordinates of A_i in the inertial frame can be computed as:

$$\mathbf{a}_i = \mathbf{p} + \mathbf{a}'_i = \mathbf{p} + \mathbf{R}^P \mathbf{a}'_i, \quad \mathbf{a}'_i = \mathbf{R}^P \mathbf{a}_i \quad (2.2)$$

For each cable, it is defined an additional fixed reference frame $D_i x_i y_i z_i$ centered in D_i . Its orientation is described in $Oxyz$ by unit vectors directed along x_i , y_i , z_i axes,

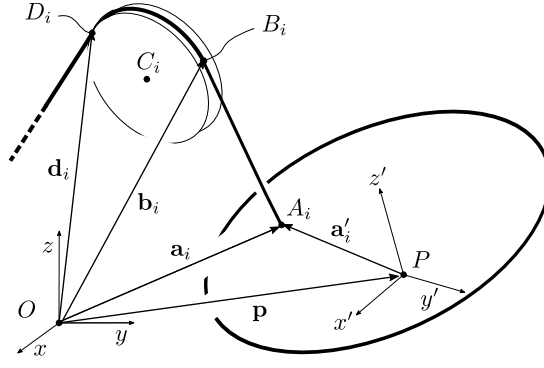


Figure 2.1: CDRP Geometric Model

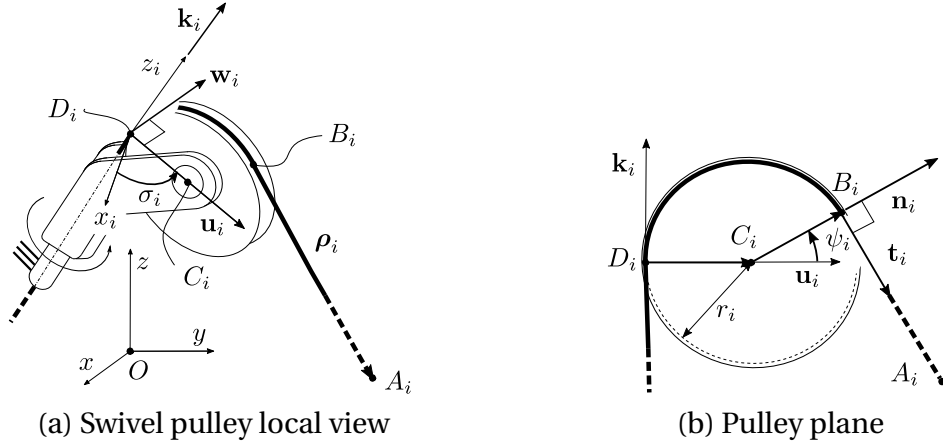


Figure 2.2: Swivel Pulley Geometric Model

namely \mathbf{i}_i , \mathbf{j}_i , \mathbf{k}_i respectively (Fig. 2.2). The *pulley plane* is defined by vectors $\boldsymbol{\rho}_i = \mathbf{a}_i - \mathbf{d}_i$ and \mathbf{k}_i

The *swivel angle* $\sigma_i \in [-\pi, \pi]$ is the angle between the coordinate plane $x_i z_i$ and the pulley plane (Fig. 2.2a). The unit vector \mathbf{w}_i normal to the *pulley plane* is:

$$\mathbf{w}_i = -\sin(\sigma_i) \mathbf{i}_i + \cos(\sigma_i) \mathbf{j}_i \quad (2.3)$$

The unit vector \mathbf{u}_i directed as $C_i - D_i$ can be calculated as $\mathbf{u}_i = \mathbf{w}_i \times \mathbf{k}_i$ or :

$$\mathbf{u}_i = \cos(\sigma_i) \mathbf{i}_i + \sin(\sigma_i) \mathbf{j}_i \quad (2.4)$$

The *tangency angle* $\psi_i \in [-\pi, \pi]$ is the angle between \mathbf{u}_i and the direction $B_i - C_i$ (Fig. 2.2a). The unit vector \mathbf{n}_i is directed as $B_i - C_i$ and can be calculated as:

$$\mathbf{n}_i = \cos(\psi_i) \mathbf{u}_i + \sin(\psi_i) \mathbf{k}_i \quad (2.5)$$

The unit vector \mathbf{t}_i is directed as $A_i - B_i$, and is calculated as $\mathbf{t}_i = \mathbf{w}_i \times \mathbf{n}_i$ or :

$$\mathbf{t}_i = \sin(\psi_i) \mathbf{u}_i - \cos(\psi_i) \mathbf{k}_i \quad (2.6)$$

Hereafter, it is discussed the relation between the parameters defined through the geometric modelling of the pulley and the direction imposed to the cable by the pulley itself.

2.1.2 First geometrical constraint on cables direction and computation of the swivel angle

The first constraint imposed by the pulley on the cable direction is defined by the equation:

$$\mathbf{w}_i \cdot \boldsymbol{\rho}_i = 0 \quad (2.7)$$

Substituting Eq. (2.3) in Eq. (2.7) yields:

$$[-\sin(\sigma_i)\mathbf{i}_i + \cos(\sigma_i)\mathbf{j}_i] \cdot \boldsymbol{\rho}_i = 0 \quad (2.8)$$

and rearranging:

$$\sin(\sigma_i)(\mathbf{i}_i \cdot \boldsymbol{\rho}_i) = \cos(\sigma_i)(\mathbf{j}_i \cdot \boldsymbol{\rho}_i) \quad (2.9)$$

thus leading to:

$$\sigma_i = \text{atan2}(\mathbf{j}_i \cdot \boldsymbol{\rho}_i, \mathbf{i}_i \cdot \boldsymbol{\rho}_i) \quad (2.10)$$

2.1.3 Second geometrical constraint on cables direction and computation of the tangency angle

We define the cable vector $\boldsymbol{\rho}_i = \mathbf{b}_i - \mathbf{a}_i$ ¹, where \mathbf{b}_i is the position vector of B_i in $Oxyz$. The second constraint imposed by the pulley on the cable direction is defined by the equation:

$$\mathbf{n}_i \cdot \boldsymbol{\rho}_i = 0 \quad (2.11)$$

If ζ is known, ψ_i can be computed from Eq. (2.11) as:

$$\boldsymbol{\rho}_i = \mathbf{a}_i - \mathbf{b}_i = \mathbf{a}_i - [\mathbf{d}_i + r_i(\mathbf{u}_i + \mathbf{n}_i)] = \boldsymbol{\rho}_i - r_i(\mathbf{u}_i + \mathbf{n}_i) \quad (2.12)$$

Substituting it in Eq. (2.11), we obtain:

$$\mathbf{n}_i \cdot [\boldsymbol{\rho}_i - r_i(\mathbf{u}_i + \mathbf{n}_i)] = \mathbf{n}_i \cdot \boldsymbol{\rho}_i - r_i(\mathbf{n}_i \cdot \mathbf{u}_i + 1) = 0 \quad (2.13)$$

Then, substituting Eq. (2.5) in Eq. (2.13) and rearranging yields:

$$\begin{aligned} (\cos(\psi_i)\mathbf{u}_i + \sin(\psi_i)\mathbf{k}_i) \cdot \boldsymbol{\rho}_i - r_i[(\cos(\psi_i)\mathbf{u}_i + \sin(\psi_i)\mathbf{k}_i) \cdot \mathbf{u}_i + 1] &= \\ = (\mathbf{u}_i \cdot \boldsymbol{\rho}_i - r_i)\cos(\psi_i) + \mathbf{k}_i \cdot \boldsymbol{\rho}_i \sin(\psi_i) - r_i &= \\ = (\varrho_{u_i} - r_i)\cos(\psi_i) + \varrho_{k_i} \sin(\psi_i) - r_i &= 0 \end{aligned} \quad (2.14)$$

where $\varrho_{k_i} = \mathbf{k}_i \cdot \boldsymbol{\rho}_i$ and $\varrho_{u_i} = \mathbf{u}_i \cdot \boldsymbol{\rho}_i$. Then, applying the following trigonometric identities:

$$\cos(\psi_i) = \frac{1 - t_i^2}{1 + t_i^2}, \quad \sin(\psi_i) = \frac{2t_i}{1 + t_i^2}, \quad t_i = \tan(\psi/2) \quad (2.15)$$

to Eq. (2.14), we obtain:

$$(\varrho_{u_i} - r_i)(1 - t_i^2) + 2\varrho_{k_i}t_i - r_i(1 + t_i^2) = -\varrho_{u_i}t_i^2 + 2\varrho_{k_i}t_i + \varrho_{u_i} - 2r_i = 0 \quad (2.16)$$

which is a second degree equation in the unknown t_i , and can be easily solved as:

$$t_i = \tan(\psi/2) = \frac{\varrho_{k_i} \pm \sqrt{(\varrho_{k_i})^2 + 1 - \frac{2r_i}{\varrho_{u_i}}}}{\varrho_{u_i}} \quad (2.17)$$

¹The use of $\boldsymbol{\rho}$ and $\boldsymbol{\rho}$ in defining position vectors $\mathbf{b}_i - \mathbf{a}_i$ and $\mathbf{d}_i - \mathbf{a}_i$ is intentional, as they are equivalent in case $r_i = 0$.

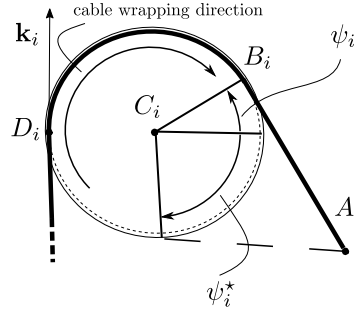


Figure 2.3: Geometric interpretation of Eq. (2.17) double solution

If the cable is clockwise wrapped onto the pulley, the only physical solution for t_i is the one with the positive sign in front of the square root (see Fig. 2.3, where the alternative solution is marked as ψ_i^*). Finally Eq. (2.18) is obtained by inverting the tan function and rearranging as:

$$\psi_i = 2 \operatorname{atan} \left[\frac{\varrho k_i}{\varrho u_i} + \sqrt{\left(\frac{\varrho k_i}{\varrho u_i} \right)^2 + 1 - \frac{2r_i}{\varrho u_i}} \right] \quad (2.18)$$

2.1.4 Geometrical constraint on cables length

Defining $l_i > 0$ as the total cable length, including both the arc $\widehat{D_i B_i} = r_i(\pi - \psi)$ wrapped onto the pulley and the rectilinear part $\|\boldsymbol{\rho}_i\|$, the geometrical constraint imposed by each cable onto the platform can be obtained. In fact, if:

$$\boldsymbol{\rho}_i = \mathbf{a}_i - \mathbf{b}_i = \boldsymbol{\varrho}_i - r_i(\mathbf{u}_i + \mathbf{n}_i) \quad (2.19)$$

and, by definition:

$$\boldsymbol{\rho}_i = [l_i - r_i(\pi - \psi)] \mathbf{t}_i = \|\boldsymbol{\rho}_i\| \mathbf{t}_i \quad (2.20)$$

where:

$$\|\boldsymbol{\rho}_i\| = l_i - r_i(\pi - \psi) \quad (2.21)$$

then we obtain the geometrical constraint:

$$\boldsymbol{\rho}_i \cdot \boldsymbol{\rho}_i - \|\boldsymbol{\rho}_i\|^2 = \boldsymbol{\rho}_i \cdot \boldsymbol{\rho}_i - [l_i - r_i(\pi - \psi)]^2 = 0 \quad (2.22)$$

In case $\boldsymbol{\zeta}$ is known, l_i can be computed from Eq. (2.22), as:

$$l_i = r_i(\pi - \psi_i) + \sqrt{\boldsymbol{\rho}_i \cdot \boldsymbol{\rho}_i} \quad (2.23)$$

2.1.5 UACDPR characterization

The obtained geometric equations are not sufficient for the characterization (and thus the control) of a generic UACDPR.

When cable lengths are assigned, Eq. (2.23), with $i = 1, \dots, n$, define the forward geometric problem, consisting in $n < 6$ equations in 6 unknowns (the elements of $\boldsymbol{\zeta}$). Such a problem is not square and, thus, undetermined.

When the *EE* configuration (the vector $\boldsymbol{\zeta}$) is assigned, Eq. (2.23), with $i = 1, \dots, n$, define the inverse geometric problem, consisting in n equations in n unknowns (cable lengths l_i). Such a problem is square and completely determined. However, the computed configuration may not be achieved in practice, since infinitely many configurations correspond to the computed cable lengths and the robot will only reach those that are compatible with mechanical equilibrium.

2.2 First order Kinematics

2.2.1 Angular velocity and twist of the EE

If the pose of the EE is described by a position vector \mathbf{p} and a rotation matrix \mathbf{R} , parametrized by a set of orientation parameters $\boldsymbol{\epsilon}$, the *angular velocity matrix* $\boldsymbol{\Omega}$ can be defined as:

$$\boldsymbol{\Omega} = \dot{\mathbf{R}}\mathbf{R}^T \quad (2.24)$$

Calculating the time derivative of the rotation matrix and rearranging yields we obtain a formula that points out that the *angular velocity vector* $\boldsymbol{\omega}$ depends non-linearly on the orientation parameter array $\boldsymbol{\epsilon}$ and linearly from its time derivative $\dot{\boldsymbol{\epsilon}}$

$$\boldsymbol{\omega} = \mathbf{H}(\boldsymbol{\epsilon})\dot{\boldsymbol{\epsilon}} \quad (2.25)$$

with:

$$\mathbf{H}(\boldsymbol{\epsilon}) = \begin{bmatrix} -c_\phi s_\theta & -s_\phi & c_\phi s_\theta \\ -s_\phi s_\theta & c_\phi & s_\phi s_\theta \\ 1 - c_\theta & 0 & c_\theta \end{bmatrix} \quad (2.26)$$

where $c_\phi = \cos(\phi)$, $s_\phi = \sin(\phi)$, $c_\theta = \cos(\theta)$ and $s_\theta = \sin(\theta)$.

The twist vector of the EE is defined as $\mathbf{v} = [\dot{\mathbf{p}}^T \boldsymbol{\omega}^T]^T$. Thus, the twist relationship with the pose $\boldsymbol{\zeta}$ and its time derivative $\dot{\boldsymbol{\zeta}}$ is given by:

$$\mathbf{v} = \mathbf{D}(\boldsymbol{\epsilon})\dot{\boldsymbol{\zeta}}, \quad \mathbf{D}(\boldsymbol{\epsilon}) = \begin{bmatrix} \mathbf{I}_{3 \times 3} & \mathbf{0}_{3 \times 3} \\ \mathbf{0}_{3 \times 3} & \mathbf{H}(\boldsymbol{\epsilon}) \end{bmatrix} \quad (2.27)$$

with $\mathbf{I}_{3 \times 3}$ and $\mathbf{0}_{3 \times 3}$ being identity and null matrices of dimension 3×3 .

2.2.2 Swivel angle time derivative

Differentiating w.r.t. Eq. (2.7) (the first constraint imposed by the pulley on the cable direction) yields:

$$\dot{\mathbf{w}}_i \cdot \boldsymbol{\rho}_i + \mathbf{w}_i \cdot \dot{\boldsymbol{\rho}}_i = 0 \quad (2.28)$$

Differentiating w.r.t. Eq. (2.2), we obtain:

$$\dot{\mathbf{a}}_i = \dot{\mathbf{p}} + \boldsymbol{\omega} \times \mathbf{a}'_i, \quad (2.29)$$

Since $\mathbf{d}_i + \boldsymbol{\rho}_i = \mathbf{a}_i$, and \mathbf{d}_i is constant in time, we may compute the velocity of point A_i as $\dot{\mathbf{a}}_i = \dot{\boldsymbol{\rho}}_i$, consequentially:

$$\dot{\boldsymbol{\rho}}_i = \dot{\mathbf{p}} + \boldsymbol{\omega} \times \mathbf{a}'_i, \quad (2.30)$$

Moreover, differentiating w.r.t. Eq. (2.3), we obtain:

$$\dot{\mathbf{w}}_i = -\dot{\sigma}_i \mathbf{u}_i \quad (2.31)$$

Substituting in Eq. (2.28) and rearranging yields:

$$\mathbf{u}_i \cdot \boldsymbol{\rho}_i \dot{\sigma}_i = \rho_{u_i} \dot{\sigma}_i = \mathbf{w}_i \cdot \dot{\mathbf{p}} + \mathbf{w}_i \cdot \boldsymbol{\omega} \times \mathbf{a}'_i = \dot{\mathbf{p}} \cdot \mathbf{w}_i + \boldsymbol{\omega} \cdot \mathbf{a}'_i \times \mathbf{w}_i \quad (2.32)$$

making the swivel angle time derivative explicit:

$$\dot{\sigma}_i = \frac{1}{\rho_{u_i}} (\dot{\mathbf{p}} \cdot \mathbf{w}_i + \boldsymbol{\omega} \cdot \mathbf{a}'_i \times \mathbf{w}_i) \quad (2.33)$$

and defining the column vector $\boldsymbol{\xi}_{\sigma_i}$, we finally obtain:

$$\dot{\sigma}_i = \boldsymbol{\xi}_{\sigma_i} \cdot \mathbf{v}, \quad \boldsymbol{\xi}_{\sigma_i} = \frac{1}{\rho_{u_i}} \begin{bmatrix} \mathbf{w}_i \\ \mathbf{a}'_i \times \mathbf{w}_i \end{bmatrix} \quad (2.34)$$

2.2.3 Tangency angle time derivative

Differentiating w.r.t. Eq. (2.11) (the second constraint imposed by the pulley on the cable direction) yields:

$$\dot{\mathbf{n}}_i \cdot \boldsymbol{\rho}_i + \mathbf{n}_i \cdot \dot{\boldsymbol{\rho}}_i = 0 \quad (2.35)$$

Its terms can be computed by differentiating w.r.t. time Eqs. (2.19), (2.4) and (2.5):

$$\dot{\boldsymbol{\rho}}_i = \dot{\mathbf{a}}_i - r_i(\dot{\mathbf{u}}_i + \dot{\mathbf{n}}_i) \quad (2.36)$$

$$\dot{\mathbf{u}}_i = \dot{\sigma}_i \mathbf{w}_i \quad (2.37)$$

$$\dot{\mathbf{n}}_i = \cos(\psi_i) \dot{\sigma}_i \mathbf{w}_i - \dot{\psi}_i \mathbf{t}_i \quad (2.38)$$

Substituting in Eq. (2.35) and rearranging yields:

$$\mathbf{t}_i \cdot \boldsymbol{\rho}_i \dot{\psi}_i = \|\boldsymbol{\rho}_i\| \dot{\psi}_i = \mathbf{n}_i \cdot \dot{\mathbf{p}} + \mathbf{n}_i \cdot \boldsymbol{\omega} \times \dot{\mathbf{a}}'_i = \dot{\mathbf{p}} \cdot \mathbf{n}_i + \boldsymbol{\omega} \cdot \dot{\mathbf{a}}'_i \times \mathbf{n}_i \quad (2.39)$$

since $\mathbf{w}_i \cdot \mathbf{n}_i = \mathbf{t}_i \cdot \mathbf{n}_i = \boldsymbol{\rho}_i \cdot \mathbf{n}_i = 0$. Finally, making the tangency angle time derivative explicit:

$$\dot{\psi}_i = \frac{1}{\|\boldsymbol{\rho}_i\|} (\dot{\mathbf{p}} \cdot \mathbf{n}_i + \boldsymbol{\omega} \cdot \dot{\mathbf{a}}'_i \times \mathbf{n}_i) \quad (2.40)$$

and defining the column vector $\boldsymbol{\xi}_{\psi_i}$, we obtain:

$$\dot{\psi}_i = \boldsymbol{\xi}_{\psi_i} \cdot \mathbf{v}, \quad \boldsymbol{\xi}_{\psi_i} = \frac{1}{\|\boldsymbol{\rho}_i\|} \begin{bmatrix} \mathbf{n}_i \\ \dot{\mathbf{a}}'_i \times \mathbf{n}_i \end{bmatrix} \quad (2.41)$$

2.2.4 Cable length time derivative

Differentiating w.r.t. time Eq. (2.22) (the geometrical constraint imposed on cables length) yields:

$$2\dot{\boldsymbol{\rho}}_i \cdot \boldsymbol{\rho}_i - 2\|\boldsymbol{\rho}_i\| \frac{\partial \|\boldsymbol{\rho}_i\|}{\partial t} = 0 \quad (2.42)$$

The time derivative of $\|\boldsymbol{\rho}_i\|$ is obtained from Eq. (2.21) as:

$$\frac{\partial \|\boldsymbol{\rho}_i\|}{\partial t} = \dot{l}_i + r_i \dot{\psi}_i \quad (2.43)$$

Substituting $\boldsymbol{\rho}_i$ (Eq. (2.20)), $\dot{\boldsymbol{\rho}}_i$ (Eq. (2.36)) and $\frac{\partial \|\boldsymbol{\rho}_i\|}{\partial t}$ (Eq. (2.43)) in Eq. (2.42) yields:

$$\|\boldsymbol{\rho}_i\| \dot{\mathbf{a}}_i \cdot \mathbf{t}_i - r_i \|\boldsymbol{\rho}_i\| [(\cos(\psi_i) + 1) \dot{\sigma}_i \mathbf{w}_i - \dot{\psi}_i \mathbf{t}_i] \cdot \mathbf{t}_i - \|\boldsymbol{\rho}_i\| (\dot{l}_i + r_i \dot{\psi}_i) = 0 \quad (2.44)$$

Simplifying and making the cable length time derivative explicit:

$$\dot{l}_i = (\dot{\mathbf{p}} \cdot \mathbf{t}_i + \boldsymbol{\omega} \cdot \dot{\mathbf{a}}'_i \times \mathbf{t}_i) \quad (2.45)$$

finally, defining the column vector $\boldsymbol{\xi}_{l_i}$, we obtain:

$$\dot{l}_i = \boldsymbol{\xi}_{l_i} \cdot \mathbf{v}, \quad \boldsymbol{\xi}_{l_i} = \begin{bmatrix} \mathbf{t}_i \\ \dot{\mathbf{a}}'_i \times \mathbf{t}_i \end{bmatrix} \quad (2.46)$$

2.2.5 Jacobian matrices

As evidenced, differentiating w.r.t. the constraint equations imposed on each cable direction and length, leads to three first order differential equations that relate the twist of the EE , respectively, to the time derivative of the swivel angle (Eq. (2.34)), the time derivative of the tangency angle (Eq. (2.41)) and the time derivative of the cable lengths (Eq. (2.46)).

All three of these equations can be written for $i = 1, \dots, n$ cables, and, defining:

$$\dot{\sigma} = [\dot{\sigma}_1 \dots, \dot{\sigma}_n]^T \quad \dot{\psi} = [\dot{\psi}_1 \dots, \dot{\psi}_n]^T \quad \dot{\mathbf{l}} = [\dot{l}_1 \dots, \dot{l}_n]^T \quad (2.47)$$

all three of these problems can be written in matrix form as:

$$\dot{\sigma} = \Xi_{\sigma} \mathbf{v}, \quad \Xi_{\sigma}^T = [\xi_{\sigma_1} \quad \dots \quad \xi_{\sigma_n}] \quad (2.48)$$

$$\dot{\psi} = \Xi_{\psi} \mathbf{v}, \quad \Xi_{\psi}^T = [\xi_{\psi_1} \quad \dots \quad \xi_{\psi_n}] \quad (2.49)$$

$$\dot{\mathbf{l}} = \Xi_l \mathbf{v}, \quad \Xi_l^T = [\xi_{l_1} \quad \dots \quad \xi_{l_n}] \quad (2.50)$$

Matrices Ξ_{σ} , Ξ_{ψ} and Ξ_l do not correlate integrable vectors (\mathbf{v} is not integrable in general), so they are kinematic Jacobians, rather than proper Jacobians. Equations (2.48) to (2.50) can be rewritten by means of proper Jacobians if we substitute therein the definition of twist given in Eq. (2.27), namely:

$$\dot{\sigma} = \mathbf{J}_{\sigma} \dot{\zeta}, \quad \mathbf{J}_{\sigma} = \Xi_{\sigma} \mathbf{D} \quad (2.51)$$

$$\dot{\psi} = \mathbf{J}_{\psi} \dot{\zeta}, \quad \mathbf{J}_{\psi} = \Xi_{\psi} \mathbf{D} \quad (2.52)$$

$$\dot{\mathbf{l}} = \mathbf{J}_l \dot{\zeta}, \quad \mathbf{J}_l = \Xi_l \mathbf{D} \quad (2.53)$$

2.3 Second order Kinematics

2.3.1 Angular acceleration and twist time derivative of the EE

Differentiating w.r.t. time Eq. (2.25), provides the analytical formulation of vector α , the *angular acceleration* of the EE :

$$\alpha = \mathbf{H}(\epsilon) \ddot{\epsilon} + \dot{\mathbf{H}}(\epsilon, \dot{\epsilon}) \dot{\epsilon}, \quad \dot{\mathbf{H}}(\epsilon, \dot{\epsilon}) = \sum_{i=1}^3 \frac{\partial \mathbf{H}(\epsilon)}{\partial \epsilon_i} \dot{\epsilon}_i \quad (2.54)$$

where:

$$\frac{\partial \mathbf{H}(\epsilon)}{\partial \epsilon_1} = \begin{bmatrix} s_{\phi} s_{\theta} & -c_{\phi} & -s_{\phi} s_{\theta} \\ -c_{\phi} s_{\theta} & -s_{\phi} & c_{\phi} s_{\theta} \\ 0 & 0 & 0 \end{bmatrix}, \quad \frac{\partial \mathbf{H}(\epsilon)}{\partial \epsilon_2} = \begin{bmatrix} -c_{\phi} c_{\theta} & 0 & c_{\phi} c_{\theta} \\ -s_{\phi} c_{\theta} & 0 & s_{\phi} c_{\theta} \\ s_{\theta} & 0 & -s_{\theta} \end{bmatrix}, \quad \frac{\partial \mathbf{H}(\epsilon)}{\partial \epsilon_3} = \mathbf{0}_{3 \times 3} \quad (2.55)$$

This result points out that α non-linearly depends on the value of the orientation parameters ϵ , it is bi-linear in $\dot{\epsilon}$, and linear in $\ddot{\epsilon}$.

The twist time derivative is thus obtained as $\dot{\mathbf{v}} = [\ddot{\mathbf{p}}^T \alpha^T]^T$, and its relationship with the pose ζ and its time derivatives $\dot{\zeta}$ and $\ddot{\zeta}$ is given by:

$$\dot{\mathbf{v}} = \mathbf{D}(\epsilon) \ddot{\zeta} + \dot{\mathbf{D}}(\epsilon, \dot{\epsilon}) \dot{\zeta}, \quad \dot{\mathbf{D}}(\epsilon, \dot{\epsilon}) = \begin{bmatrix} \mathbf{0}_{3 \times 3} & \mathbf{0}_{3 \times 3} \\ \mathbf{0}_{3 \times 3} & \dot{\mathbf{H}}(\epsilon, \dot{\epsilon}) \end{bmatrix} \quad (2.56)$$

2.3.2 Swivel angle second order time derivative

The rate of change $\dot{\sigma}_i$ of the swivel-angle time-derivative can be computed from the time derivative of Eq. (2.34) as:

$$\ddot{\sigma}_i = \xi_{\sigma_i} \cdot \dot{\mathbf{v}} + \dot{\xi}_{\sigma_i} \cdot \mathbf{v} \quad (2.57)$$

Hereafter will be discussed an alternative method to compute swivel-angle second order time-derivative. Considering Eq. (2.28) and substituting Eq. (2.31) and $\dot{\rho}_i = \dot{\mathbf{a}}_i$, yields:

$$\mathbf{u}_i \rho_i \dot{\sigma}_i = \mathbf{w}_i \cdot \dot{\mathbf{a}}_i \quad (2.58)$$

Deriving Eq. (2.58) w.r.t. time leads to:

$$[\dot{\mathbf{u}}_i \cdot \rho_i + \mathbf{u}_i \cdot \dot{\rho}_i] \dot{\sigma}_i + \rho_{u_i} \ddot{\sigma}_i = \dot{\mathbf{w}}_i \cdot \dot{\mathbf{a}}_i + \mathbf{w}_i \cdot \ddot{\mathbf{a}}_i \quad (2.59)$$

and accounting for Eqs. (2.7), (2.29) and:

$$\ddot{\mathbf{a}}_i = \ddot{\mathbf{p}} + \boldsymbol{\alpha} \times \mathbf{a}'_i + \boldsymbol{\omega} \times (\boldsymbol{\omega} \times \mathbf{a}'_i) \quad (2.60)$$

one has:

$$\ddot{\sigma}_i = -\frac{2}{\rho_{u_i}} (\xi_{u_i} \cdot \mathbf{v}) (\xi_{\sigma_i} \cdot \mathbf{v}) + \xi_{\sigma_i} \cdot \dot{\mathbf{v}} + \frac{\mathbf{w}_i}{\rho_{u_i}} \cdot \boldsymbol{\omega} \times (\boldsymbol{\omega} \times \mathbf{a}'_i), \quad \xi_{u_i} = \begin{bmatrix} \mathbf{u}_i \\ \mathbf{a}'_i \times \mathbf{u}_i \end{bmatrix} \quad (2.61)$$

The Jacobi identity of the vector product allows us to write the formula:

$$\mathbf{w}_i \cdot \boldsymbol{\omega} \times (\boldsymbol{\omega} \times \mathbf{a}'_i) = \boldsymbol{\omega} \cdot \mathbf{a}'_i \times (\mathbf{w}_i \times \boldsymbol{\omega}) \quad (2.62)$$

Eq. (2.61) can be rewritten in matrix form as:

$$\ddot{\sigma}_i = \mathbf{v}^T \xi'_{\sigma_i} \mathbf{v} + \xi_{\sigma_i}^T \dot{\mathbf{v}} \quad (2.63)$$

where:

$$\xi'_{\sigma_i} = \frac{1}{\rho_{u_i}} (-2\xi_{u_i} \xi_{\sigma_i}^T + \mathbf{A}_{w_i}), \quad \mathbf{A}_{w_i} = \begin{bmatrix} \mathbf{0}_{3 \times 3} & \mathbf{0}_{3 \times 3} \\ \mathbf{0}_{3 \times 3} & \tilde{\mathbf{a}}'_i \tilde{\mathbf{w}}_i \end{bmatrix} \quad (2.64)$$

Finally, comparing Eqs. (2.57) and (2.63), one can obtain:

$$\dot{\xi}_{\sigma_i} = \xi'_{\sigma_i} \mathbf{v} \quad (2.65)$$

2.3.3 Tangency angle second order time derivative

The rate of change $\dot{\psi}_i$ of the tangency-angle time-derivative can be computed from the time derivative of Eq. (2.41) as:

$$\ddot{\psi}_i = \xi_{\psi_i} \cdot \mathbf{v} + \dot{\xi}_{\psi_i} \cdot \dot{\mathbf{v}} \quad (2.66)$$

Hereafter will be discussed an alternative method to compute tangency-angle second order time-derivative. Considering Eq. (2.35) and substituting Eq. (2.38) and $\dot{\rho}_i = \dot{\mathbf{a}}_i - r_i(\dot{\mathbf{u}}_i + \dot{\mathbf{n}}_i)$, yields:

$$\|\rho_i\| \dot{\psi}_i = \mathbf{n}_i \cdot \dot{\mathbf{a}}_i \quad (2.67)$$

Deriving w.r.t. time Eq. (2.67) one obtains:

$$\frac{\partial \|\boldsymbol{\rho}_i\|}{\partial t} \dot{\psi}_i + \|\boldsymbol{\rho}_i\| \ddot{\psi}_i = \dot{\mathbf{n}}_i \cdot \dot{\mathbf{a}}_i + \mathbf{n}_i \cdot \ddot{\mathbf{a}}_i \quad (2.68)$$

and accounting for Eqs. (2.38) and (2.43), one has:

$$\ddot{\psi}_i = \frac{1}{\|\boldsymbol{\rho}_i\|} (\varrho_{u_i} \cos(\psi_i) \dot{\sigma}_i^2 - r_i \dot{\psi}_i^2 - 2\dot{l}_i \dot{\psi}_i + \mathbf{n}_i \cdot \boldsymbol{\omega} \times (\boldsymbol{\omega} \times \mathbf{a}'_i)) + \boldsymbol{\xi}_{\psi_i} \cdot \dot{\mathbf{v}} \quad (2.69)$$

The Jacobi identity of the vector product allows us to write the formula:

$$\mathbf{n}_i \cdot \boldsymbol{\omega} \times (\boldsymbol{\omega} \times \mathbf{a}'_i) = \boldsymbol{\omega} \cdot \mathbf{a}'_i \times (\mathbf{n}_i \times \boldsymbol{\omega}) \quad (2.70)$$

Using Eqs. (2.34), (2.41) and (2.46), Eq. (2.61) can be rewritten in matrix form as:

$$\ddot{\psi}_i = \mathbf{v}^T \boldsymbol{\xi}'_{\psi_i} \mathbf{v} + \boldsymbol{\xi}_{\psi_i}^T \dot{\mathbf{v}} \quad (2.71)$$

where:

$$\boldsymbol{\xi}'_{\psi_i} = \frac{1}{\|\boldsymbol{\rho}_i\|} \left(\varrho_{u_i} \cos(\psi_i) \boldsymbol{\xi}_{\sigma_i} \boldsymbol{\xi}_{\sigma_i}^T - r_i \boldsymbol{\xi}_{\psi_i} \boldsymbol{\xi}_{\psi_i}^T - 2\boldsymbol{\xi}_{l_i} \boldsymbol{\xi}_{\psi_i}^T + \mathbf{A}_{n_i} \right), \quad \mathbf{A}_{n_i} = \begin{bmatrix} \mathbf{0}_{3 \times 3} & \mathbf{0}_{3 \times 3} \\ \mathbf{0}_{3 \times 3} & \mathbf{a}'_i \mathbf{n}_i \end{bmatrix} \quad (2.72)$$

Finally, comparing Eqs. (2.66) and (2.71), one can obtain:

$$\dot{\boldsymbol{\xi}}_{\psi_i} = \boldsymbol{\xi}'_{\psi_i} \mathbf{v} \quad (2.73)$$

2.3.4 Cable-length second order time derivative

The rate of change \ddot{l}_i of the cable-length time-derivative can be computed from the time-derivative of Eq. (2.46) as:

$$\ddot{l}_i = \dot{\boldsymbol{\xi}}_{l_i} \cdot \mathbf{v} + \boldsymbol{\xi}_{l_i} \cdot \dot{\mathbf{v}} \quad (2.74)$$

Hereafter will be discussed an alternative method to compute cable-length second order time-derivative. Substituting Eq. (2.29) into Eq. (2.45) yields:

$$\dot{l}_i = \dot{\mathbf{a}}_i \cdot \mathbf{t}_i \quad (2.75)$$

Deriving Eq. (2.75) w.r.t. time leads to:

$$\ddot{l}_i = \dot{\mathbf{t}}_i \cdot \dot{\mathbf{a}}_i + \mathbf{t}_i \cdot \ddot{\mathbf{a}}_i \quad (2.76)$$

where $\dot{\mathbf{t}}_i$ is obtained deriving w.r.t. time Eq. (2.6):

$$\dot{\mathbf{t}}_i = \sin(\psi_i) \dot{\sigma}_i \mathbf{w}_i + \dot{\psi}_i \mathbf{n}_i \quad (2.77)$$

Then, substituting Eq. (2.77), (2.29) and (2.60) into Eq. (2.76), one has:

$$\ddot{l}_i = \sin(\psi_i) \varrho_{u_i} \dot{\sigma}_i^2 + \|\boldsymbol{\rho}_i\| \dot{\psi}_i^2 + \mathbf{t}_i \cdot \boldsymbol{\omega} \times (\boldsymbol{\omega} \times \mathbf{a}'_i) + \boldsymbol{\xi}_{l_i} \cdot \dot{\mathbf{v}} \quad (2.78)$$

The Jacobi identity of the vector product allows us to write the formula:

$$\mathbf{t}_i \cdot \boldsymbol{\omega} \times (\boldsymbol{\omega} \times \mathbf{a}'_i) = \boldsymbol{\omega} \cdot \mathbf{a}'_i \times (\mathbf{t}_i \times \boldsymbol{\omega}) \quad (2.79)$$

Using Eqs. (2.34), (2.41) and (2.79), Eq. (2.78) can be rewritten in matrix form as:

$$\ddot{l}_i = \mathbf{v}^T \boldsymbol{\xi}'_{l_i} \mathbf{v} + \boldsymbol{\xi}_{l_i}^T \dot{\mathbf{v}} \quad (2.80)$$

where:

$$\boldsymbol{\xi}'_{l_i} = \sin(\psi_i) \varrho_{u_i} \boldsymbol{\xi}_{\sigma_i} \boldsymbol{\xi}_{\sigma_i}^T + \|\boldsymbol{\rho}_i\| \boldsymbol{\xi}_{\psi_i} \boldsymbol{\xi}_{\psi_i}^T + \mathbf{A}_{t_i}, \quad \mathbf{A}_{t_i} = \begin{bmatrix} \mathbf{0}_{3 \times 3} & \mathbf{0}_{3 \times 3} \\ \mathbf{0}_{3 \times 3} & \mathbf{a}'_i \dot{\mathbf{t}}_i \end{bmatrix} \quad (2.81)$$

Finally, comparing Eqs. (2.74) and (2.80), one can obtain:

$$\dot{\boldsymbol{\xi}}_{l_i} = \boldsymbol{\xi}'_{l_i} \mathbf{v} \quad (2.82)$$

2.4 EE free and controlled kinematics

2.4.1 Controlled and free pose-coordinates

The number of *DoFs* of *UACDPRs* being strictly greater than the number n of their actuators is a feature that unavoidably leads them to be underactuated, even if all cables are taut, all kinematic constraints are active and kinematic Jacobian matrix Ξ_l in Eq. (2.50) has full rank. From a controllistic point of view, one notices that modifying cable lengths, only n coordinates of the *EE* pose can be piloted, while the remaining $\lambda = 6 - n$ are to be determined. Moreover, if actuators are locked (which means that cable lengths are kept constant), λ freedoms remain. The n controlled coordinates will be referred to as *controlled pose-coordinates* and denoted as $\zeta_c \in \mathbb{R}^n$, whereas the non-controllable coordinates will be referred to as *free pose-coordinates* and denoted as $\zeta_f \in \mathbb{R}^\lambda$. In addition, a 6×6 permutation matrix² \mathbf{P} is introduced, so that the array of permuted *EE* generalized coordinates, ζ_p , and its time-derivatives are defined as:

$$\zeta_p = \begin{bmatrix} \zeta_c \\ \zeta_f \end{bmatrix} = \mathbf{P}\zeta, \quad \dot{\zeta}_p = \mathbf{P}\dot{\zeta}, \quad \ddot{\zeta}_p = \mathbf{P}\ddot{\zeta} \quad (2.83)$$

The analysis of the direct geometric problem arising from Eq. (2.23) for $i = 1 \dots n$, shows up that the controlled pose-coordinates are determinable as a function of the cable lengths \mathbf{l} (the system controlled variables) and the free-pose coordinates ζ_f .

$$\zeta_c = \zeta_c(\zeta_f, \mathbf{l}) \quad (2.84)$$

It should be noted that this problem is under-determined, since the value of the free pose-coordinates ζ_f is not assignable. However, their evolution can be determined by the mechanical equilibrium of the *UACDPR*.

2.4.2 Free twist and free pose-coordinates derivative

The *EE* twist \mathbf{v} can be decomposed into two contributions, a *free twist* \mathbf{v}_f and a *controlled twist* \mathbf{v}_c , so that:

$$\mathbf{v} = \mathbf{v}_f + \mathbf{v}_c \quad (2.85)$$

The *free twist* is defined as the *EE* twist when the platform is in free motion, namely when cable lengths remain constant in time. Substituting $\dot{\mathbf{l}} = \mathbf{0}_{n \times 1}$ into Eq. (2.50), yields:

$$\Xi_l \mathbf{v}_f = \mathbf{0}_{n \times 1} \quad (2.86)$$

This kind of equation can be solved considering the right nullspace $\Xi_l^{\perp T}$ of matrix Ξ_l , i.e. a $(6 \times \lambda)$ matrix such that $\Xi_l \Xi_l^{\perp T} = \mathbf{0}_{n \times \lambda}$. Indeed, its columns define a basis for the free twist \mathbf{v}_f :

$$\mathbf{v}_f = \Xi_l^{\perp T} \mathbf{c} \quad \text{for some } \mathbf{c} \in \mathbb{R}^\lambda \quad (2.87)$$

Similarly, substituting $\dot{\mathbf{l}} = \mathbf{0}_{n \times 1}$ into Eq. (2.53), yields:

$$\mathbf{J}_l \dot{\zeta} = \mathbf{0}_{n \times 1} \quad (2.88)$$

²A permutation matrix is an orthogonal matrix, that has exactly one entry of 1 in each row and each column, and has 0's elsewhere.

and, considering the right nullspace $\mathbf{J}_l^{\perp T}$ of matrix \mathbf{J}_l , we obtain a solution:

$$\dot{\boldsymbol{\zeta}} = \mathbf{J}_l^{\perp T} \mathbf{c}' \quad \text{for some } \mathbf{c}' \in \mathbb{R}^\lambda \quad (2.89)$$

When the platform is in free motion $\mathbf{v}_c = 0$, thus $\mathbf{v} = \mathbf{v}_f$, and so, Eq. (2.27) becomes:

$$\mathbf{v}_f = \mathbf{D}\dot{\boldsymbol{\zeta}} = \mathbf{D}\mathbf{J}_l^{\perp T} \mathbf{c}' \quad \text{for some } \mathbf{c}' \in \mathbb{R}^\lambda \quad (2.90)$$

By comparing Eqs. (2.87) and (2.90) and by choosing $\mathbf{c} = \mathbf{c}'$, we have:

$$\boldsymbol{\Xi}_l^{\perp T} = \mathbf{D}\mathbf{J}_l^{\perp T} \quad (2.91)$$

Hereafter it is proved that, when matrix $\boldsymbol{\Xi}_l^{\perp T}$ (and thus $\mathbf{J}_l^{\perp T}$) is computed according to a specified procedure, the coefficients \mathbf{c} coincide with the free-pose coordinates derivative $\dot{\boldsymbol{\zeta}}_f$. First, we define the permuted Jacobian matrix \mathbf{J}_P as:

$$\mathbf{J}_P = \mathbf{J}_l \mathbf{P}^T = \boldsymbol{\Xi}_l \mathbf{D} \mathbf{P}^T = \boldsymbol{\Xi}_l [\mathbf{D}_c \quad \mathbf{D}_f] = [\mathbf{J}_c \quad \mathbf{J}_f] \quad (2.92)$$

where $\mathbf{D}_c \in \mathbb{R}^{6 \times n}$, $\mathbf{D}_f \in \mathbb{R}^{6 \times \lambda}$, $\mathbf{J}_c = \boldsymbol{\Xi}_l \mathbf{D}_c \in \mathbb{R}^{n \times n}$, and $\mathbf{J}_f = \boldsymbol{\Xi}_l \mathbf{D}_f \in \mathbb{R}^{n \times \lambda}$. Then, defining the permuted right nullspace matrix as:

$$\mathbf{J}_P^\perp = \mathbf{J}_l^\perp \mathbf{P}^T \quad (2.93)$$

the right nullspace of the permuted Jacobian matrix $\mathbf{J}_P^{\perp T}$ can be obtained by the definition of right nullspace of the Jacobian matrix:

$$\mathbf{J}_l \mathbf{J}_l^{\perp T} = \mathbf{J}_P \mathbf{P} \mathbf{P}^T \mathbf{J}_P^{\perp T} = \mathbf{J}_P \mathbf{J}_P^{\perp T} = \mathbf{0}_{n \times \lambda} \quad (2.94)$$

Matrix \mathbf{J}_P^\perp can be symbolically computed substituting Eq. (2.92) into Eq. (2.94), under the assumption that \mathbf{J}_c is full rank (namely, $\text{rank}(\mathbf{J}_c) = n$).

$$[\mathbf{J}_c \quad \mathbf{J}_f] \mathbf{J}_P^{\perp T} = \mathbf{0}, \quad \mathbf{J}_P^{\perp T} = \begin{bmatrix} -\mathbf{J}_c^{-1} \mathbf{J}_f \\ \mathbf{I}_{\lambda \times \lambda} \end{bmatrix} \quad (2.95)$$

In case of free motion, with $\ddot{\mathbf{I}} = 0$, Eq. (2.53) also provides a symbolic formulation of vector $\dot{\boldsymbol{\zeta}}_p$ as a function of vector $\dot{\boldsymbol{\zeta}}_f$.

$$\mathbf{J}_l \dot{\boldsymbol{\zeta}} = \mathbf{J}_P \mathbf{P} \mathbf{P}^T \dot{\boldsymbol{\zeta}}_p = \mathbf{J}_P \dot{\boldsymbol{\zeta}}_p = \mathbf{J}_c \dot{\boldsymbol{\zeta}}_c + \mathbf{J}_f \dot{\boldsymbol{\zeta}}_f = \mathbf{0}_{n \times 1} \quad (2.96)$$

Then:

$$\dot{\boldsymbol{\zeta}}_c = -\mathbf{J}_c^{-1} \mathbf{J}_f \dot{\boldsymbol{\zeta}}_f \quad (2.97)$$

and finally:

$$\dot{\boldsymbol{\zeta}}_p = \begin{bmatrix} \dot{\boldsymbol{\zeta}}_c \\ \dot{\boldsymbol{\zeta}}_f \end{bmatrix} = \begin{bmatrix} -\mathbf{J}_c^{-1} \mathbf{J}_f \\ \mathbf{I}_{\lambda \times \lambda} \end{bmatrix} \dot{\boldsymbol{\zeta}}_f = \mathbf{J}_P^{\perp T} \dot{\boldsymbol{\zeta}}_f \quad (2.98)$$

In the end, one has:

$$\mathbf{v}_f = \mathbf{D}\dot{\boldsymbol{\zeta}} = \mathbf{D} \mathbf{P}^T \dot{\boldsymbol{\zeta}}_p = \mathbf{D} \mathbf{P}^T \mathbf{J}_P^{\perp T} \dot{\boldsymbol{\zeta}}_f = \mathbf{D} \mathbf{J}_l^{\perp T} \dot{\boldsymbol{\zeta}}_f = \boldsymbol{\Xi}_l^{\perp T} \dot{\boldsymbol{\zeta}}_f \quad (2.99)$$

And, finally comparing Eqs. (2.87) and (2.99), we obtain $\mathbf{c} = \dot{\boldsymbol{\zeta}}_f$.

Chapter 3

Initial Pose Estimation Problem

A major issue in the practical use of *UACDPRs* is the estimation of the *EE* pose when the machine is turned on. In a generic start-up condition, cable lengths and the *EE* pose are unknown and have to be determined in order to start performing any desired operation.

External measurement devices such as laser trackers [15] or high-resolution cameras [16] can be employed to measure the *EE* pose, and the corresponding cable lengths can be easily computed from Eq. 2.23. Having accurate knowledge of the initial cable lengths is critical because, for *CDPRs* equipped with relative encoders, the initial lengths are used to compute the absolute cable lengths. Absolute cable lengths are then used to determine the *EE* pose through direct kinematics. Consequently, inaccuracies in the computation of the initial length would result in errors in the determination of robot poses as the robot moves for performing tasks.

Alternatively, in order to collect kinematic data, one can use a set of proprioceptive measurement devices, namely a set of sensors that measure some of the *EE* pose parameters or some of the internal joint variables of the robot and thereby determine the initial cable lengths and the initial pose of the *EE*. This approach is generally referred to as *self-calibration* or *internal-calibration* [10, 17, 18].

In [12] an automatic procedure to estimate the initial pose of a generic suspended under-actuated *CDPR* that only relies on incremental measurements of length and orientation is proposed and a data acquisition procedure is defined. The article shows how, if the *UACDPR* is equipped with incremental encoders on motors and on swivel axes, the variation of cable lengths and swivel angles at a generic equilibrium pose can be measured relative to the initial values of cable lengths and swivel angles. If data are acquired in different equilibrium poses an overdetermined system of equations can be written and solved as a non-linear least-square optimization.

The disadvantage of this method is that the equations involved are based on data collected in static configurations. *UACDPRs* are underconstrained robots and, when moved from one equilibrium configuration to another, they exhibit oscillatory free motion. This means that for proper data acquisition, one should wait until the oscillatory motion has been fully damped whenever the equilibrium configuration is changed.

The goal of the first part of this work is to find a variation of the method that allows data on cable length and orientation to be collected during the free motion of the platform, in order to reduce the acquisition time.

3.1 Initial Pose Estimation Problem with Incremental Encoders

In this chapter, the initial cable length estimation problem will be formulated by extending the work presented in [12]. Under-actuated manipulators, if excited by an external impulse, exhibit an oscillatory behavior even if all their actuators are locked, that is *free-motion*. The initial-pose estimation problem will be formulated taking advantage of this particular feature of *UACDPRs*.

3.1.1 Modelling

In the following, a 6-*DoFs* n -cable *UACDPR* equipped with measurement devices is considered. Incremental encoders on the swivel axes of the n pulleys are employed in order to measure the development of variation of swivel angles $\Delta\sigma_i$, for $i = 1, \dots, n$ during free-motion. If measures are sampled with some chosen frequency, to each reached pose ζ_k correspond n measures $\Delta\sigma_i^k$. In a generic pose ζ_k reached during the oscillatory motion, swivel angles can be computed as a non-linear function of the pose $\sigma_k(\zeta_k) = [\sigma_1^k(\zeta_k), \dots, \sigma_n^k(\zeta_k)]^T$ (Eqs. 2.10), or as the sum of the initial offset on swivel angles $\sigma^0 = [\sigma_1^0, \dots, \sigma_n^0]^T$ and measured k -th variations on swivel angles $\Delta\sigma^k = [\Delta\sigma_1^k, \dots, \Delta\sigma_n^k]^T$, namely:

$$\sigma(\zeta_k) = \sigma^0 + \Delta\sigma^k \quad (3.1)$$

Moreover, cable lengths can be computed as a non-linear function of the generic pose $\mathbf{l}_k(\zeta_k) = [l_1(\zeta_k), \dots, l_n(\zeta_k)]^T$ (Eq. 2.23), or, considering that actuators are locked, can be set equal to their initial values $\mathbf{l}^0 = [l_1^0, \dots, l_n^0]^T$, namely:

$$\mathbf{l}(\zeta_k) = \mathbf{l}^0 \quad (3.2)$$

Rearranging and regrouping Eqs. 3.1 and 3.2 in a vector \mathbf{F}_k , function of the unknowns $\zeta_k, \sigma^0, \mathbf{l}^0$:

$$\mathbf{F}_k(\zeta_k, \sigma^0, \mathbf{l}^0) = \begin{bmatrix} \sigma(\zeta_k) - \sigma^0 - \Delta\sigma^k \\ \mathbf{l}(\zeta_k) - \mathbf{l}^0 \end{bmatrix} = \mathbf{0} \quad (3.3)$$

The key-idea of this method is to make use, as well as of the geometric constraints equations (Eqs. 3.3), also of the first order kinematic equations on cable lengths (Eqs. 2.53). Setting $\dot{\mathbf{l}} = \mathbf{0}$, we have, for every pose ζ_k of the oscillatory free-motion:

$$\mathbf{J}_l \dot{\zeta}_k = \mathbf{0} \quad (3.4)$$

where matrix \mathbf{J}_l depends as well on the platform pose ζ_k (Eqs. 2.53).

If measures are sampled at sufficiently high frequency, vector $\dot{\zeta}_k$ can be approximated to backward finite differences (App. A). In order to express the approximated vector in a closed form, the order of accuracy N has to be chosen, and a $6 \times (N + 1)$ matrix \mathbf{Z}_k has to be defined:

$$\mathbf{Z}_k = [\zeta_{k-N}, \zeta_{k-N+1}, \dots, \zeta_k] \quad (3.5)$$

also, the coefficients vector \mathbf{C} has to be computed as the solution of the linear system A.9. Thus, results:

$$\dot{\zeta}_k \simeq \frac{1}{h} \mathbf{Z}_k \mathbf{C} \quad (3.6)$$

where h is the time spacing between two consecutive acquisitions, namely the inverse of sampling rate. Eqs. 3.4 can be finally rewritten as:

$$\mathbf{J}_l \frac{1}{h} \mathbf{Z}_k \mathbf{C} = \mathbf{0} \quad (3.7)$$

and regrouped in a vector \mathbf{G}_k , function of the unknowns:

$$\mathbf{G}_k(\mathbf{Z}_k) = \mathbf{J}_l(\zeta_k) \mathbf{Z}_k \mathbf{C} = \mathbf{0} \quad (3.8)$$

By assuming that λ different measurement sets are available, λ equations $\mathbf{F}_k = \mathbf{0}$ and $\lambda - N$ equations $\mathbf{G}_k = \mathbf{0}$ can be written, thus leading to the system of equations:

$$\mathbf{F}_k(\zeta_k, \boldsymbol{\sigma}^0, \mathbf{l}^0) = \begin{bmatrix} \boldsymbol{\sigma}(\zeta_k) - \boldsymbol{\sigma}^0 - \Delta \boldsymbol{\sigma}^k \\ \mathbf{l}(\zeta_k) - \mathbf{l}^0 \end{bmatrix} = \mathbf{0} \quad k = 1, \dots, \lambda \quad (3.9)$$

$$\mathbf{G}_k(\mathbf{Z}_k) = \mathbf{J}_l(\zeta_k) \mathbf{Z}_k \mathbf{C} = \mathbf{0} \quad k = N + 1, \dots, \lambda \quad (3.10)$$

or, in another form:

$$\mathbf{F}_k(\zeta_k, \boldsymbol{\sigma}^0, \mathbf{l}^0) = \begin{bmatrix} \boldsymbol{\sigma}(\zeta_k) - \boldsymbol{\sigma}^0 - \Delta \boldsymbol{\sigma}^k \\ \mathbf{l}(\zeta_k) - \mathbf{l}^0 \end{bmatrix} = \mathbf{0} \quad k = 1, \dots, N \quad (3.11)$$

$$\mathbf{H}_k(\mathbf{Z}_k, \boldsymbol{\sigma}^0, \mathbf{l}^0) = \begin{bmatrix} \boldsymbol{\sigma}(\zeta_k) - \boldsymbol{\sigma}^0 - \Delta \boldsymbol{\sigma}^k \\ \mathbf{l}(\zeta_k) - \mathbf{l}^0 \\ \mathbf{J}_l(\zeta_k) \mathbf{Z}_k \mathbf{C} = \mathbf{0} \end{bmatrix} = \mathbf{0} \quad k = N + 1, \dots, \lambda \quad (3.12)$$

This is a system of $n(3\lambda - N)$ equations in $2n + 6\lambda$ unknowns, where $\mathbf{X} = [\zeta_1, \dots, \zeta_\lambda, \boldsymbol{\sigma}^0, \mathbf{l}^0]$ is the vector of the unknowns. Thus, chosen the order of the approximation N , if $\lambda > \frac{n(2+N)}{3n-6}$ the initial-pose estimation problem is overdetermined and can be formulated as a non-linear least-square optimization. This problem can be solved by employing numerical techniques, such as the Trust-region-reflective algorithm. To find an efficient solution to this optimization problem, it is necessary to determine a reasonable initial solution guess $\mathbf{X}_{\text{guess}}$, which is fundamental for both solution accuracy and algorithm speed, as well as an analytical formulation of the Jacobian matrix, which is crucial for having relatively short computation times.

3.1.2 Simulation Results

Simulations are performed in MATLAB® on a 6-DoF *EE* suspended by 4 cables. For the *UACDPR* used for simulations, the platform mass is $m = 1\text{kg}$, the reference point P on the *EE* is the center of gravity and the transmission properties are summarized in Tables 3.1, 3.2. Running several simulations has shown how $500 < \lambda < 2200$ dif-

i	$\mathbf{d}_i[\text{m}]$	$r_i[\text{m}]$	${}^P \mathbf{a}'_i[\text{m}]$
1	$[1.5, 1.0, 0.0]^T$	0	$[0.10, 0.15, 0.15]^T$
2	$[1.5, -1.0, 0.0]^T$	0	$[0.10, -0.15, 0.15]^T$
3	$[-1.5, -1.0, 0.0]^T$	0	$[-0.10, -0.15, 0.15]^T$
4	$[-1.5, 1.0, 0.0]^T$	0	$[-0.10, 0.15, 0.15]^T$

Table 3.1: Actuation unit properties 1

i	\mathbf{x}_i	\mathbf{y}_i	\mathbf{z}_i
1	$[-0.018, 1.000, 0.018]^T$	$[0.013, 0.018, -1.000]^T$	$[-1.000, -0.018, -0.013]^T$
2	$[-1.000, 0.005, -0.006]^T$	$[0.005, -0.028, -1.000]^T$	$[-0.006, -1.000, 0.028]^T$
3	$[0.006, -1.000, 0.006]^T$	$[-0.014, -0.006, -1.000]^T$	$[1.000, 0.006, -0.014]^T$
4	$[1.000, -0.020, -0.019]^T$	$[-0.020, -0.010, -1.000]^T$	$[0.019, 1.000, -0.010]^T$

Table 3.2: Actuation unit properties 2

ferent measurement sets, sampled with frequency $f_c = 100\text{Hz}$ lead to optimal results. To the best of the author knowledge, such data sets contain enough information for the algorithm to converge, without being too wide, affecting the algorithm with inaccuracies resulting from the inversion of very large matrices and becoming critical to solve in terms of computational time. Also, simulations are performed assuming that incremental encoders on the swivel axes are affected by a measurement random error of maximum amplitude $\text{err}_{\Delta\sigma} = 0.5^\circ$, and that the initial solution guess $\mathbf{X}_{\text{guess}}$ differs from the exact solution \mathbf{X} by 10%. The order of accuracy of backward finite difference chosen is $N = 7$.

The first simulations have been carried out considering to excite the platform and acquiring measures in $\lambda = 500$ different points, when the platform is swinging around the center of the workspace (Config. P_0 , Fig. 3.1). In Fig. 3.2 percentage and absolute cable lengths errors are reported. Of all the algorithm unknowns it was chosen to show only the results concerning cable lengths, that are the most important results of the procedure. In fact, for given cable lengths, it is always possible to compute the *EE* pose by solving a so-called *Geometrico-Static Problem* [12], or, if measurements of the pitch and roll angles are available, by the direct kinematics solution proposed in Chapter 4. It is clear that the algorithm does not converge to the solution, the maximum percentage error in fact is even greater than the error on the initial guess.

Secondly, simulations have been carried out considering to excite the platform and acquire measures in $\lambda = 600$ different points, when the platform is swinging around 3 different points in the workspace: specifically in 3 central points vertically aligned (Config. A , Fig. 3.3), and in 3 points lying on the same horizontal central plane (Config. B , Fig. 3.5). In moving from one configuration to another incremental encoders on central axes of pulleys acquire measures of cable lengths variations. The following simulations are performed assuming that those encoders are affected by a measurement random error that cause an error in measured cable lengths variations of maximum amplitude $\text{err}_{\Delta l} = 4\text{mm}$. In Figs. 3.4, 3.6 percentage and absolute cable lengths errors are reported. Those simulations prove that if measures are acquired exciting the platform in different points at different heights results improve. But even in this case, the algorithm does not converge, because the maximum percentage error is still larger than the error on the initial guess. Also, the results show that acquiring measures exciting the platform in different points at the same height brings no benefits, in fact the maximum percentage error remains around 25%.

Finally, simulations have been carried out considering to excite the platform and acquire measures in $\lambda = 1200$ different points, when the platform is swinging around 6 different points, the centre of the workspace and 5 points lying on an horizontal lower plane (Config. C , Fig. 3.7), and in $\lambda = 2200$ different points, when the platform is swinging around 11 different points, the centre of the workspace and 10 points lying on two

horizontal lower planes (Config. D , Fig. 3.9). In Figs. 3.8, 3.10 percentage and absolute cable lengths errors are reported, showing that the algorithm accuracy does not significantly increase if measure are acquired in more than 6 points. Results are again unusable, in fact a maximum absolute error of 2cm would lead to inadmissible inaccuracies in the computation of the EE pose.

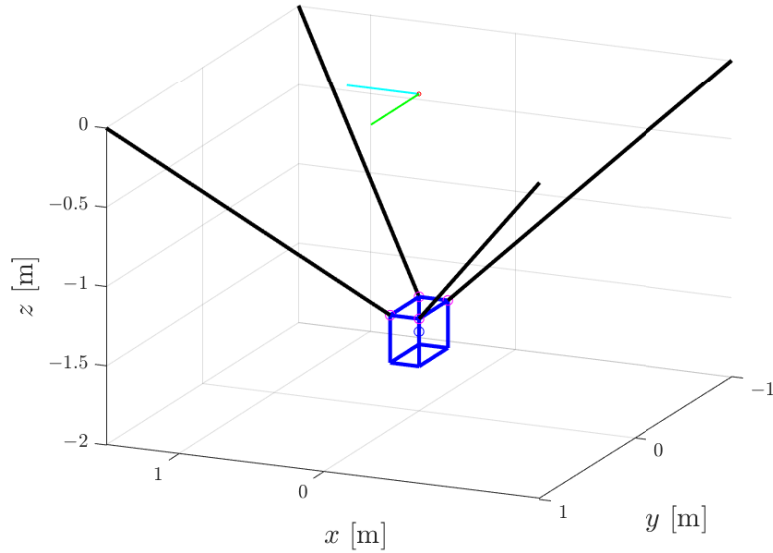


Figure 3.1: Config. P_0

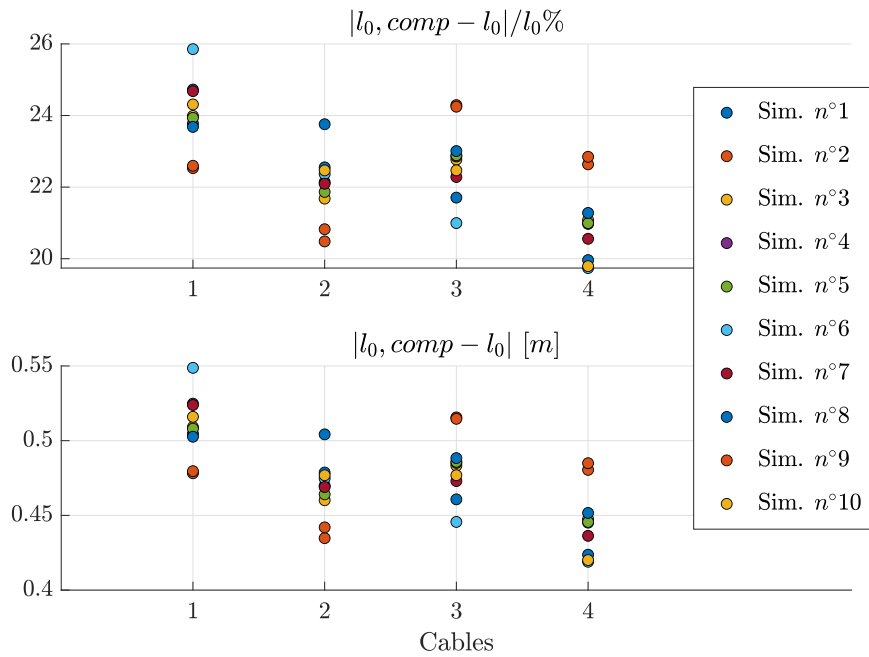


Figure 3.2: Percentage and absolute solution error for measures acquired in Config. P_0

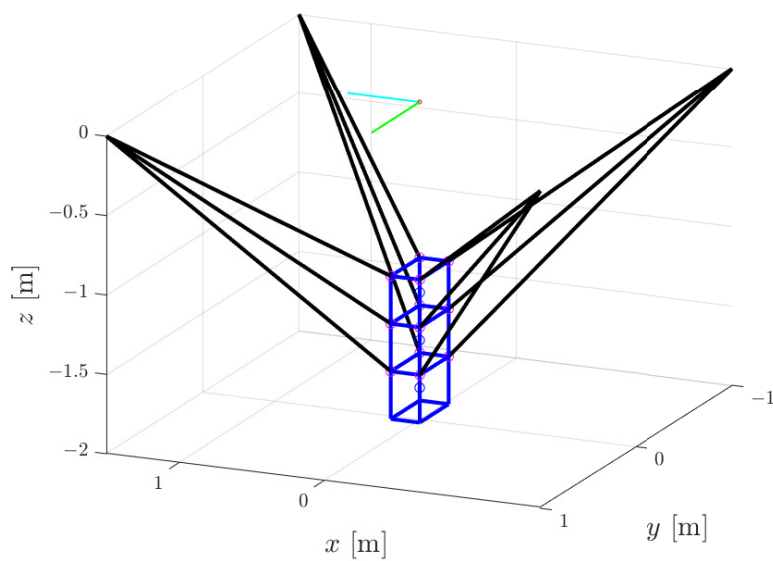


Figure 3.3: Config. A

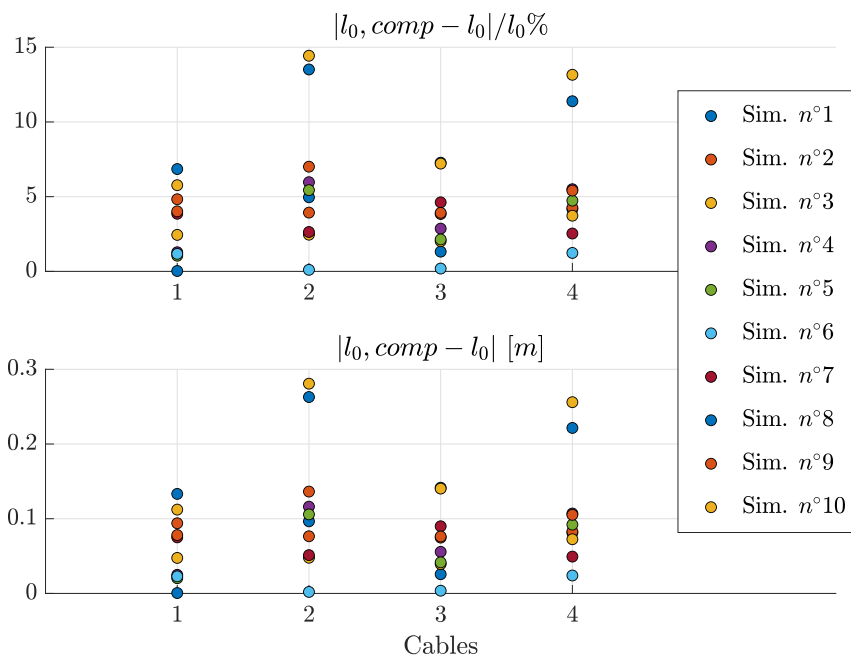


Figure 3.4: Percentage and absolute solution error for measures acquired in Config. A

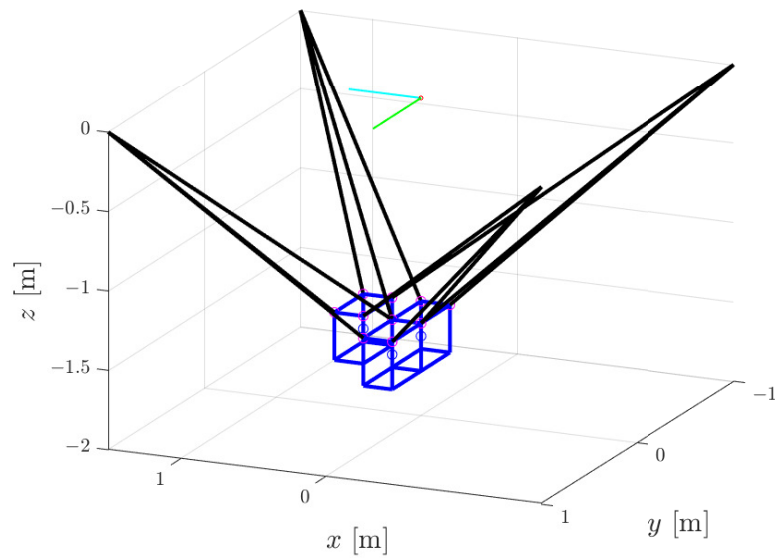


Figure 3.5: Config. *B*

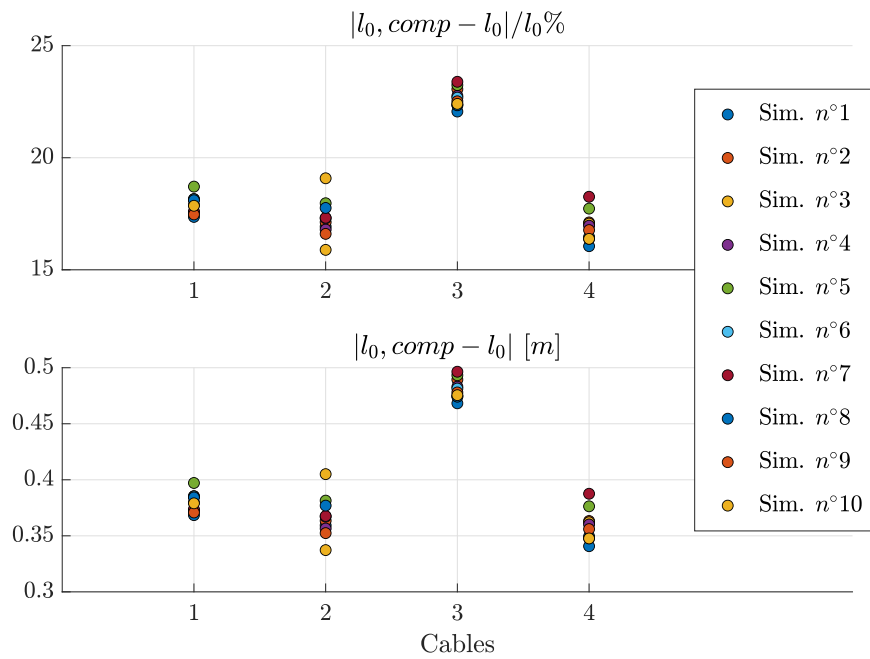


Figure 3.6: Percentage and absolute solution error for measures acquired in Config. *B*

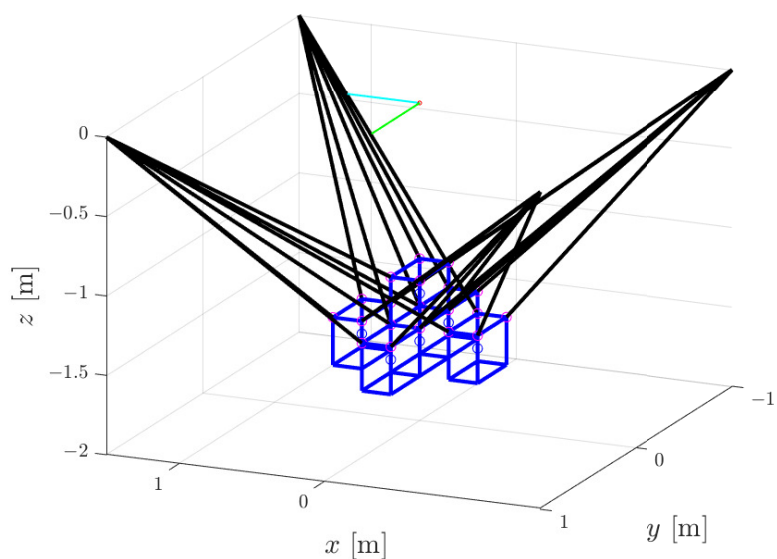


Figure 3.7: Config. C

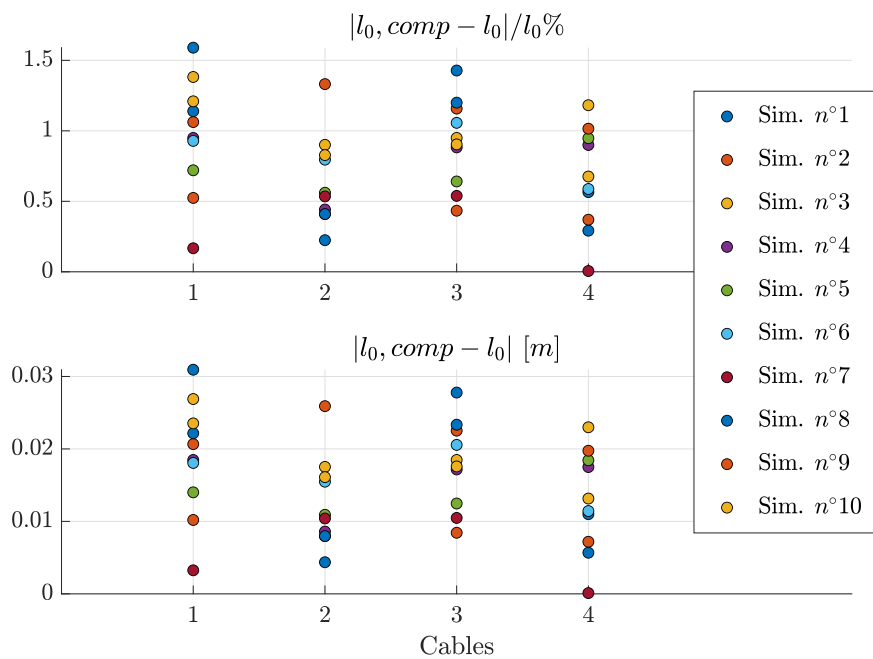


Figure 3.8: Percentage and absolute solution error for measures acquired in Config. C

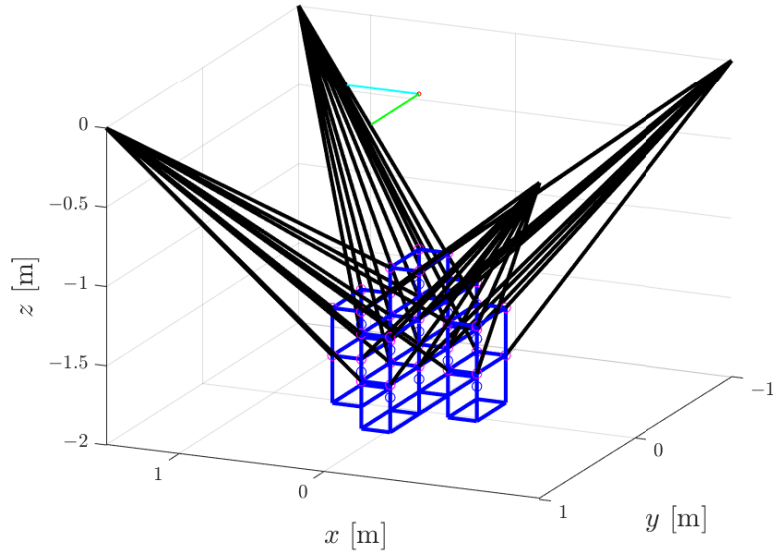


Figure 3.9: Config. *D*

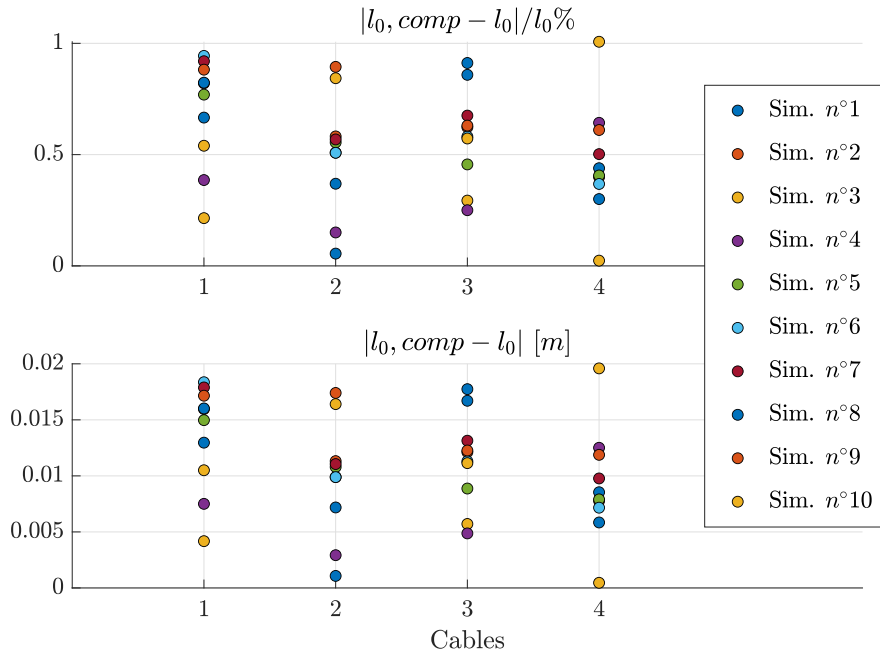


Figure 3.10: Percentage and absolute solution error for measures acquired in Config. *D*

3.2 Initial Pose Estimation Problem with Absolute Encoders

In this Chapter, absolute encoders placed on swivel axes measuring swivel angles during free-motion are considered in place of incremental encoders. This approach is proposed as an alternative to the one discussed in Chapter 3.1.

3.2.1 Modelling

In the following, a 6-DoFs n -cable UACDPR equipped with absolute encoders is considered. These devices are mounted on the swivel axes of the n pulleys and are used to measure the development of swivel angles σ_i , for $i = 1, \dots, n$ during free-motion. If measures are sampled, to each reached pose ζ_k correspond n measures σ_i^k . In a generic pose ζ_k reached during the oscillatory motion, swivel angles, which can be expressed as a non-linear function of the pose $\sigma_k(\zeta_k) = [\sigma_1^k(\zeta_k), \dots, \sigma_n^k(\zeta_k)]^T$ (Eqs. 2.10), are equal to the k -th measures $\sigma^k = [\sigma_1^k, \dots, \sigma_n^k]^T$, namely:

$$\sigma(\zeta_k) = \sigma^k \quad (3.13)$$

Eq. 3.2 holds true for cable lengths, and, rearranged and combined with equation 3.13 in a vector \mathbf{F}_k , yields to the following system of equations, in the unknowns ζ_k, \mathbf{I}^0 :

$$\mathbf{F}_k(\zeta_k, \mathbf{I}^0) = \begin{bmatrix} \sigma(\zeta_k) - \sigma^k \\ \mathbf{l}(\zeta_k) - \mathbf{l}^0 \end{bmatrix} = \mathbf{0} \quad (3.14)$$

First order kinematic equations on cable lengths (Eqs. 2.53), approximated to backward finite difference (App. A) with order of accuracy N , with $\dot{\mathbf{l}} = \mathbf{0}$, are taken into account and regrouped in a vector \mathbf{G}_k function of the unknowns:

$$\mathbf{G}_k(\mathbf{Z}_k) = \mathbf{J}_l(\zeta_k) \mathbf{Z}_k \mathbf{C} = \mathbf{0} \quad (3.15)$$

where \mathbf{C} is a vector of coefficients (computed as the solution of the linear system A.9) and matrix \mathbf{Z}_k is:

$$\mathbf{Z}_k = [\zeta_{k-N}, \zeta_{k-N+1}, \dots, \zeta_k] \quad (3.16)$$

By assuming that λ different measurement sets are available, λ equations $\mathbf{F}_k = \mathbf{0}$ and $\lambda - N$ equations $\mathbf{G}_k = \mathbf{0}$ can be written, thus leading to the system of equations:

$$\mathbf{F}_k(\zeta_k, \mathbf{I}^0) = \begin{bmatrix} \sigma(\zeta_k) - \sigma^k \\ \mathbf{l}(\zeta_k) - \mathbf{l}^0 \end{bmatrix} = \mathbf{0} \quad k = 1, \dots, \lambda \quad (3.17)$$

$$\mathbf{G}_k(\mathbf{Z}_k) = \mathbf{J}_l(\zeta_k) \mathbf{Z}_k \mathbf{C} = \mathbf{0} \quad k = N + 1, \dots, \lambda \quad (3.18)$$

or, in another form:

$$\mathbf{F}_k(\zeta_k, \mathbf{I}^0) = \begin{bmatrix} \sigma(\zeta_k) - \sigma^k \\ \mathbf{l}(\zeta_k) - \mathbf{l}^0 \end{bmatrix} = \mathbf{0} \quad k = 1, \dots, N \quad (3.19)$$

$$\mathbf{H}_k(\mathbf{Z}_k, \mathbf{I}^0) = \begin{bmatrix} \sigma(\zeta_k) - \sigma^k \\ \mathbf{l}(\zeta_k) - \mathbf{l}^0 \\ \mathbf{J}_l(\zeta_k) \mathbf{Z}_k \mathbf{C} = \mathbf{0} \end{bmatrix} = \mathbf{0} \quad k = N + 1, \dots, \lambda \quad (3.20)$$

This is a system of $n(3\lambda - N)$ equations in $n + 6\lambda$ unknowns, where $\mathbf{X} = [\zeta_1, \dots, \zeta_\lambda, \mathbf{I}^0]$ is the vector of the unknowns. Thus, chosen the order of the approximation N , if

$\lambda > \frac{n(1+N)}{3n-6}$ the initial-pose estimation problem is overdetermined and can be formulated as a non-linear least-square optimization. This problem can be solved by means of numerical techniques, such as the Trust-region-reflective algorithm. Again, the efficiency of the algorithm depends on both the accuracy of the initial solution vector \mathbf{X}_{guess} and the analytic formulation of the Jacobian matrix, while the accuracy of the solution depends only on the accuracy of \mathbf{X}_{guess} .

3.2.2 Simulation Results

Simulations are performed in MATLAB® on a 6-DoF EE suspended by 4 cables. For the UACDPR used for simulations, the platform mass is $m = 1\text{kg}$, the reference point P on the EE is the center of gravity and the transmission properties are summarized in Tables 3.1, 3.2. The simulation parameters are the same chosen in Subsec. 3.1.2. $500 < \lambda < 2200$ different measurement sets have been acquired, sampled with frequency $f_c = 100\text{Hz}$. Also, simulations are performed assuming that incremental encoders on central axes of pulleys are affected by a measurement random error that causes an error in measured cable lengths variations of maximum amplitude $\text{err}_{\Delta l} = 4\text{mm}$. The initial solution guess \mathbf{X}_{guess} differs from the exact solution \mathbf{X} by 10% and the order of accuracy of backward finite difference is $N = 7$. In this Section, measures on swivel axes are acquired by absolute encoders, which are supposed to be affected by a measurement random error of maximum amplitude $\text{err}_{\sigma} = 0.5^\circ$.

Simulations have been carried out exciting the platform and acquiring measures in $\lambda = 500$ different points when the platform is swinging around the center of the workspace (Config. P_0 , Fig. 3.1), and in the best-case scenarios resulting from simulations performed in Subsec. 3.1.2, namely when the platform is excited and measures are acquired:

- in $\lambda = 600$ different points, when the platform is swinging around 3 central points vertically aligned (Config. A, 3.3)
- in $\lambda = 1200$ different points, when the platform is swinging around 6 different points, the center of the workspace and 5 points lying on a horizontal lower plane (Config. C, Fig. 3.7)
- in $\lambda = 2200$ different points, when the platform is swinging around 11 different points, the center of the workspace and 10 points lying on two horizontal lower planes (Config. D, Fig. 3.9)

In Figs. 3.11, 3.12, 3.13, 3.14 percentage and absolute cable lengths errors resulting from the simulations performed are reported. Results show that if swivel angles are measured with absolute encoders, rather than with incremental encoders (Subsec. 3.1.2), the accuracy of the algorithm improves for data acquired in one or few points in the workspace, and gets worse for data acquired in multiple points in the workspace. However, it still leads to huge errors in the determination of cable lengths.

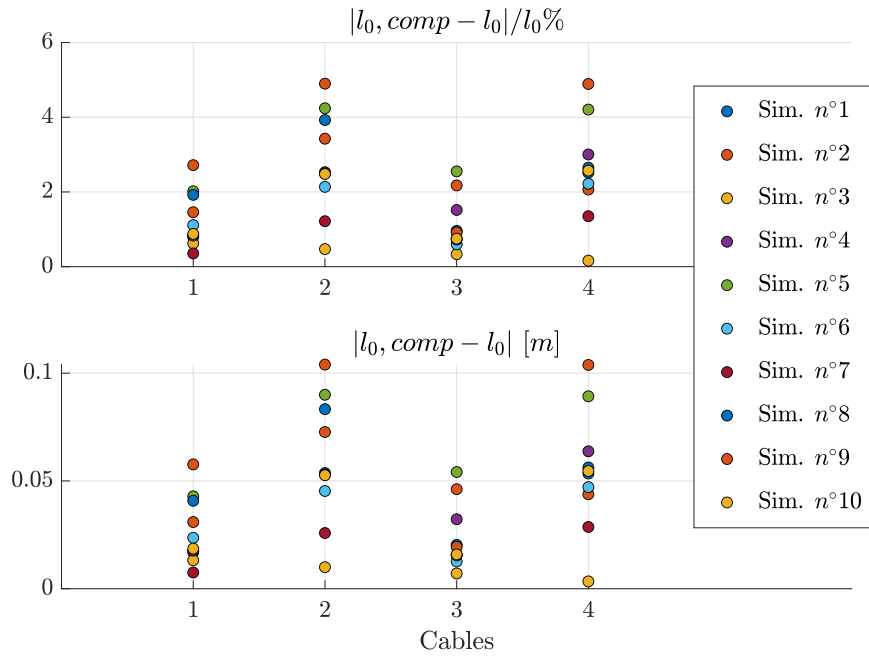


Figure 3.11: Percentage and absolute solution error for measures acquired in Config. P_0

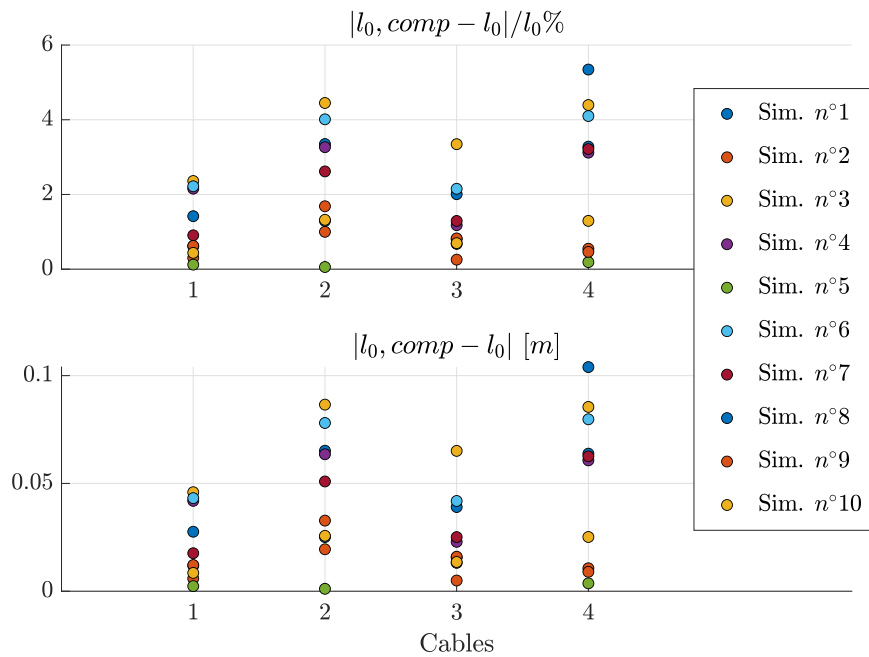


Figure 3.12: Percentage and absolute solution error for measures acquired in Config. A

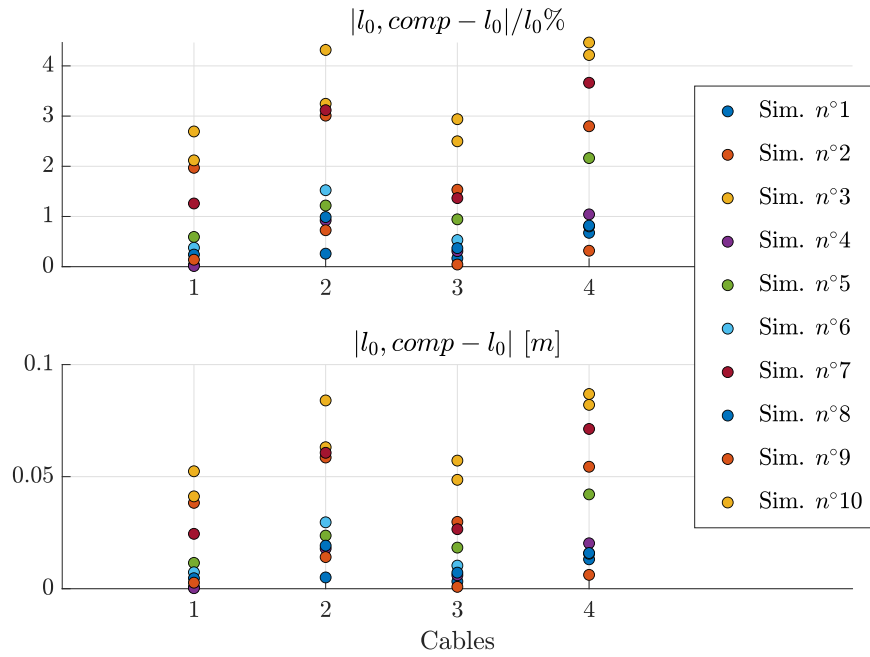


Figure 3.13: Percentage and absolute solution error for measures acquired in Config. C

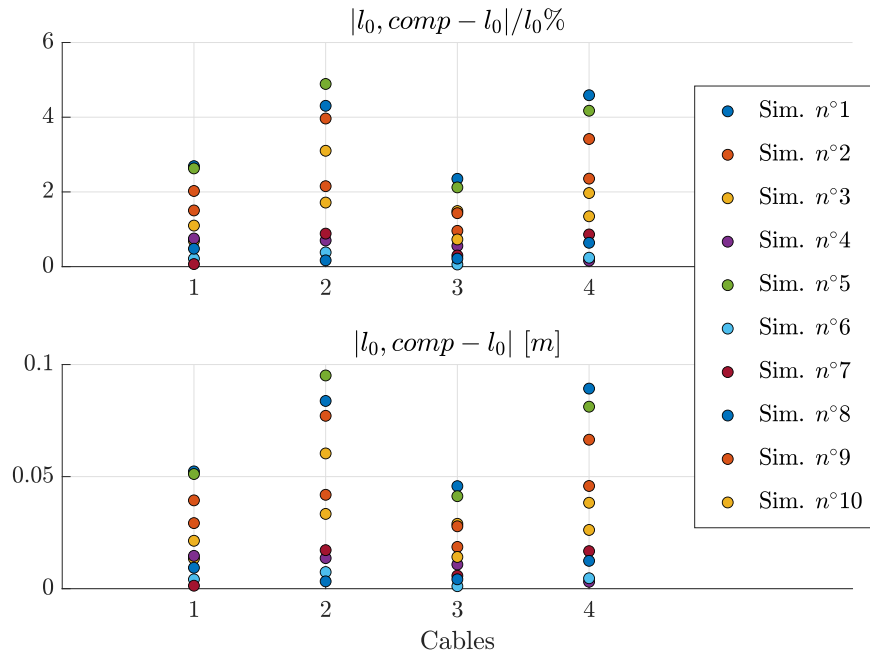


Figure 3.14: Percentage and absolute solution error for measures acquired in Config. D

3.3 Initial Pose Estimation Problem with Incremental Encoders and Inclinometers on the Platform

As an alternative to the approach proposed in Section 3.1, one can consider adding sensors that directly measure some pose parameters or other model variables. The use of additional sensors for solving the direct kinematics of *CDPRs* is widely discussed in the literature [10, 12, 19]. As shown in Section 3.1, swivel-pulley angles are good extra-measurement candidates, due to their ease of implementation and generally good accuracy. Merlet [10] experimentally showed that measuring some orientation parameters of the *EE* with static inclinometers (i.e. accelerometers) provides acceptable results for static postures and quasi-static motions. In this work the platform is excited by an external impulse, exhibiting an oscillatory behavior. If the amplitude of the impulse is sufficiently small (and it must be for the cables to stay taut), we may suppose that inclinometers fixed on the platform provide as well accurate measures of some of the pose parameters.

3.3.1 Modelling

In the following, a 6-*DoFs* *n*-cable *UACDPR* equipped with measurement devices is considered. Incremental encoders on the swivel axes of the *n* pulleys are employed in order to measure the development of variation of swivel angles $\Delta\sigma_i$, for $i = 1, \dots, n$ during free-motion. As shown in Subsection 3.1.1 this set of measurements and the dependence of swivel angles and cable lengths on the pose ζ_k , lead to the system of equations:

$$\sigma(\zeta_k) - \sigma^0 - \Delta\sigma^k = \mathbf{0} \quad (3.21)$$

$$\mathbf{l}(\zeta_k) - \mathbf{l}^0 = \mathbf{0} \quad (3.22)$$

If inclinometers measuring the development of pitch and roll angles of the *EE* are added as measurement devices, two of the pose-parameters are no longer unknowns of the problem but extra reliable data, the knowledge of which could improve the performances of the numerical solver. Thus, the *EE* pose is divided in *known-parameters*, the pitch θ and the roll ϕ , and *unknown-parameters*, the *EE* position \mathbf{p} and the yaw angle ψ , that remain unknowns for our initial pose estimation problem. Choosing as *free pose-coordinates* (ζ_f) (2.4) the subset of pose parameters measured by dynamic inclinometers, the remaining subset, namely the unknown-parameters, are set as the *controlled pose-coordinates* (ζ_c). Expressing equations 3.22 as a function of the problem unknowns leads to:

$$\mathbf{F}_k(\zeta_{k,c}, \sigma^0, \mathbf{l}^0) = \begin{bmatrix} \sigma(\zeta_k) - \sigma^0 - \Delta\sigma^k \\ \mathbf{l}(\zeta_k) - \mathbf{l}^0 \end{bmatrix} = \mathbf{0} \quad (3.23)$$

Moreover, for every pose ζ_k , holds Eq. 2.83, and, making ζ_k explicit we obtain:

$$\zeta_k = \mathbf{P}^T \zeta_{k,P} = \mathbf{P}^T \begin{bmatrix} \zeta_{k,c} \\ \zeta_{k,f} \end{bmatrix} \quad (3.24)$$

and, consequently:

$$\dot{\zeta}_k = \mathbf{P}^T \begin{bmatrix} \dot{\zeta}_{k,c} \\ \dot{\zeta}_{k,f} \end{bmatrix} \quad (3.25)$$

Also, manipulating Eq. 2.92 yields:

$$\mathbf{J}_l = \mathbf{J}_P \mathbf{P} = [\mathbf{J}_c \quad \mathbf{J}_f] \mathbf{P} \quad (3.26)$$

Substituting Eqs. 3.25 and 3.26 into the first-order kinematic equations on cable lengths (Eqs. 2.53) and setting $\dot{\mathbf{l}} = \mathbf{0}$:

$$[\mathbf{J}_c \quad \mathbf{J}_f] \mathbf{P} \mathbf{P}^T \begin{bmatrix} \dot{\boldsymbol{\zeta}}_{k,c} \\ \dot{\boldsymbol{\zeta}}_{k,f} \end{bmatrix} = \mathbf{0} \quad (3.27)$$

whereas \mathbf{P} is a permutation matrix (see Sec. 2.4), hence $\mathbf{P} \mathbf{P}^T = \mathbf{I}_{6 \times 6}$, thus leading to:

$$\mathbf{J}_c \dot{\boldsymbol{\zeta}}_{k,c} + \mathbf{J}_f \dot{\boldsymbol{\zeta}}_{k,f} = \mathbf{0} \quad (3.28)$$

Matrices \mathbf{J}_c and \mathbf{J}_f are composed of columns of matrix \mathbf{J}_l , thus they also depend on the platform pose $\boldsymbol{\zeta}_k$ (Eqs. 2.53). If measures are sampled at sufficiently high frequency, vectors $\dot{\boldsymbol{\zeta}}_{k,c}$ and $\dot{\boldsymbol{\zeta}}_{k,f}$ can be approximated to backward finite differences (App. A). Chosen the order of accuracy of the approximation N , and defined two $6 \times (N+1)$ matrices $\mathbf{Z}_{k,c}$ and $\mathbf{Z}_{k,f}$ such that:

$$\mathbf{Z}_{k,c} = [\boldsymbol{\zeta}_{k-N,c}, \quad \boldsymbol{\zeta}_{k-N+1,c}, \quad \dots, \quad \boldsymbol{\zeta}_{k,c}] \quad (3.29)$$

$$\mathbf{Z}_{k,f} = [\boldsymbol{\zeta}_{k-N,f}, \quad \boldsymbol{\zeta}_{k-N+1,f}, \quad \dots, \quad \boldsymbol{\zeta}_{k,f}] \quad (3.30)$$

so that:

$$\mathbf{Z}_k = [\boldsymbol{\zeta}_{k-N}, \quad \boldsymbol{\zeta}_{k-N+1}, \quad \dots, \quad \boldsymbol{\zeta}_k] = \mathbf{P}^T \begin{bmatrix} \mathbf{Z}_{k,c} \\ \mathbf{Z}_{k,f} \end{bmatrix} \quad (3.31)$$

Eqs. 3.28 can be finally rewritten as:

$$\mathbf{J}_c \frac{1}{h} \mathbf{Z}_{k,c} \mathbf{C} + \mathbf{J}_f \frac{1}{h} \mathbf{Z}_{k,f} \mathbf{C} = \mathbf{0} \quad (3.32)$$

where h is the time spacing between two consecutive acquisitions and \mathbf{C} is the coefficients vector (computed as the solution of the linear system A.9). Finally, Eq. 3.32 can be regrouped in a vector \mathbf{G}_k , function of the unknowns, namely the matrix of the controlled pose coordinates $\mathbf{Z}_{k,c}$:

$$\mathbf{G}_k(\mathbf{Z}_{k,c}) = \mathbf{J}_c \mathbf{Z}_{k,c} \mathbf{C} + \mathbf{J}_f \mathbf{Z}_{k,f} \mathbf{C} = \mathbf{0} \quad (3.33)$$

By assuming that λ different measurement sets are available, λ equations $\mathbf{F}_k = \mathbf{0}$ and $\lambda - N$ equations $\mathbf{G}_k = \mathbf{0}$ can be written, thus leading to the system of equations:

$$\mathbf{F}_k(\boldsymbol{\zeta}_{k,c}, \boldsymbol{\sigma}^0, \mathbf{l}^0) = \begin{bmatrix} \boldsymbol{\sigma}(\boldsymbol{\zeta}_k) - \boldsymbol{\sigma}^0 - \Delta \boldsymbol{\sigma}^k \\ \mathbf{l}(\boldsymbol{\zeta}_k) - \mathbf{l}^0 \end{bmatrix} = \mathbf{0} \quad k = 1, \dots, \lambda \quad (3.34)$$

$$\mathbf{G}_k(\mathbf{Z}_{k,c}) = \mathbf{J}_c \mathbf{Z}_{k,c} \mathbf{C} + \mathbf{J}_f \mathbf{Z}_{k,f} \mathbf{C} = \mathbf{0} \quad k = N+1, \dots, \lambda \quad (3.35)$$

or, in another form:

$$\mathbf{F}_k(\boldsymbol{\zeta}_{k,c}, \boldsymbol{\sigma}^0, \mathbf{l}^0) = \begin{bmatrix} \boldsymbol{\sigma}(\boldsymbol{\zeta}_k) - \boldsymbol{\sigma}^0 - \Delta \boldsymbol{\sigma}^k \\ \mathbf{l}(\boldsymbol{\zeta}_k) - \mathbf{l}^0 \end{bmatrix} = \mathbf{0} \quad k = 1, \dots, N \quad (3.36)$$

$$\mathbf{H}_k(\mathbf{Z}_{k,c}, \boldsymbol{\sigma}^0, \mathbf{l}^0) = \begin{bmatrix} \boldsymbol{\sigma}(\boldsymbol{\zeta}_k) - \boldsymbol{\sigma}^0 - \Delta \boldsymbol{\sigma}^k \\ \mathbf{l}(\boldsymbol{\zeta}_k) - \mathbf{l}^0 \\ \mathbf{J}_c \mathbf{Z}_{k,c} \mathbf{C} + \mathbf{J}_f \mathbf{Z}_{k,f} \mathbf{C} = \mathbf{0} \end{bmatrix} = \mathbf{0} \quad k = N+1, \dots, \lambda \quad (3.37)$$

This is a system of $n(3\lambda - N)$ equations in $2n + 4\lambda$ unknowns. $\mathbf{X} = [\zeta_{1,c}, \dots, \zeta_{\lambda,c}, \sigma^0, \mathbf{1}^0]$ is the vector of the unknowns. Thus, chosen the order of the approximation N , if $\lambda > \frac{n(2+N)}{3n-4}$ the initial-pose estimation problem is overdetermined and can be formulated as a non-linear least-square optimization. As for the problem in Chapter 3.1, the solution can be computed by means of the Trust-region-reflective algorithm, determining a reasonable initial solution guess \mathbf{X}_{guess} and an analytical formulation of the Jacobian matrix.

3.3.2 Simulation Results

Simulations are performed in MATLAB® on a 6-DoF *EE* suspended by 4 cables. For the *UACDPR* used for simulations, the platform mass is $m = 1\text{kg}$, the reference point P on the *EE* is the center of gravity and the transmission properties are summarized in Tables 3.1, 3.2. The simulation parameters are the same chosen in Subsec. 3.1.2. $500 < \lambda < 2200$ different measurement sets have been acquired, sampled with frequency $f_c = 100\text{Hz}$. Also, simulations are performed assuming that incremental encoders on swivel axes are affected by a measurement random error of maximum amplitude $\text{err}_{\Delta\sigma} = 0.5^\circ$, and that incremental encoders on central axes of pulleys cause an error in measured cable lengths variations of maximum amplitude $\text{err}_{\Delta l} = 4\text{mm}$. The initial solution guess \mathbf{X}_{guess} differs from the exact solution \mathbf{X} by 10% and the order of accuracy of backward finite difference is $N = 7$. In this Section, measures are acquired also by static inclinometers. We assume that errors on those measures are random from a normal distribution with mean parameter 0 and standard deviation parameter $\text{err}_{\zeta_f} = 0.2^\circ$.

Simulations have been carried out exciting the platform and acquiring measures when the platform is swinging around the center of the workspace (Config. P_0 , Fig. 3.1), and in the best-case scenarios resulting from simulations performed in Subsec. 3.1.2, namely when the platform is excited and measures are acquired:

- in $\lambda = 600$ different points, when the platform is swinging around 3 central points vertically aligned (Config. *A*, 3.3)
- in $\lambda = 1200$ different points, when the platform is swinging around 6 different points, the center of the workspace and 5 points lying on a horizontal lower plane (Config. *C*, Fig. 3.7)
- in $\lambda = 2200$ different points, when the platform is swinging around 11 different points, the center of the workspace and 10 points lying on two horizontal lower planes (Config. *D*, Fig. 3.9)

In Fig. 3.15 percentage and absolute cable length errors resulting from the first set of simulations are reported. Even in this case, with measures acquired in only one point of the workspace, the algorithm clearly does not converge. In Figs. 3.16, 3.17, 3.18 percentage and absolute cable lengths errors resulting from the simulations listed above are reported. Results show how the algorithm accuracy slightly improves providing pitch-and-roll extra-measurements; still, remains unusable: a maximum absolute error of 1cm leads to significant inaccuracies in the computation of the *EE* pose. Even if measures are acquired in 11 different points in the workspace (Config. *D*) cable-lengths are determined with a maximum percentage error of 0.5% (Fig. 3.18), that, compared with the maximum percentage error of 1.0% (Fig. 3.10) obtained without

inclinometers (Sec. 3.1), is not a result that can justify the costs associated with the purchase of inclinometers.

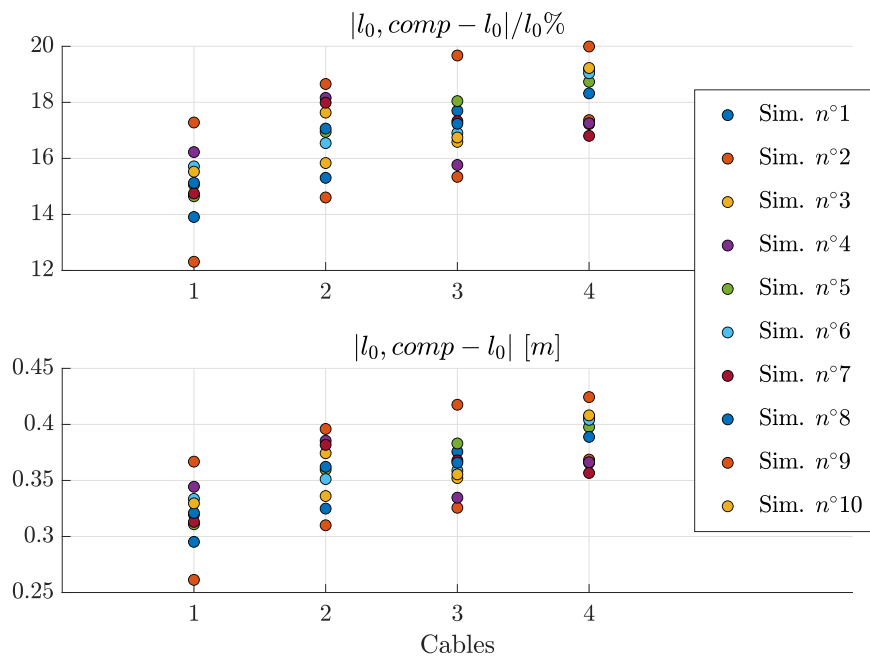


Figure 3.15: Percentage and absolute solution error for measures acquired in Config. P_0

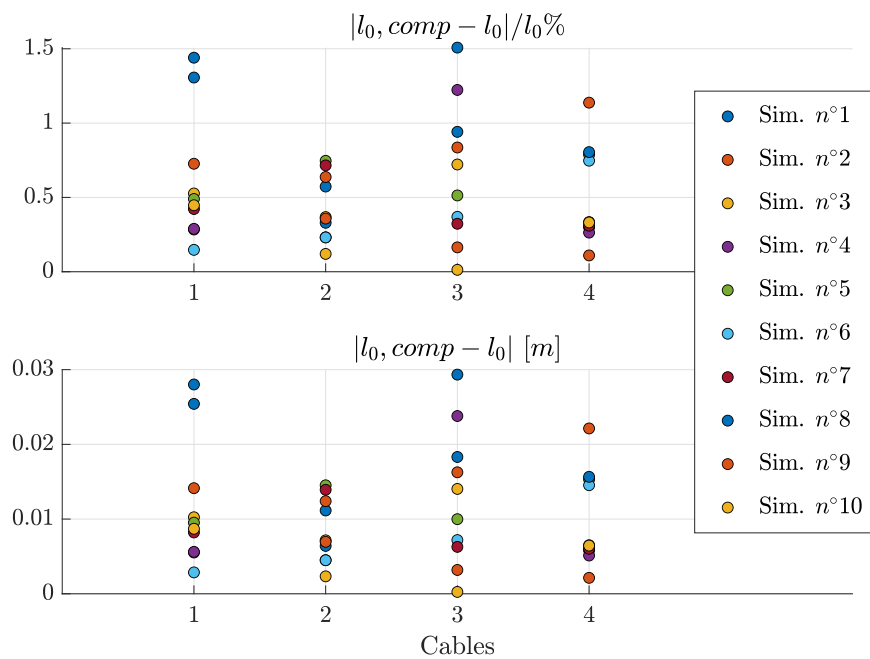


Figure 3.16: Percentage and absolute solution error for measures acquired in Config. A

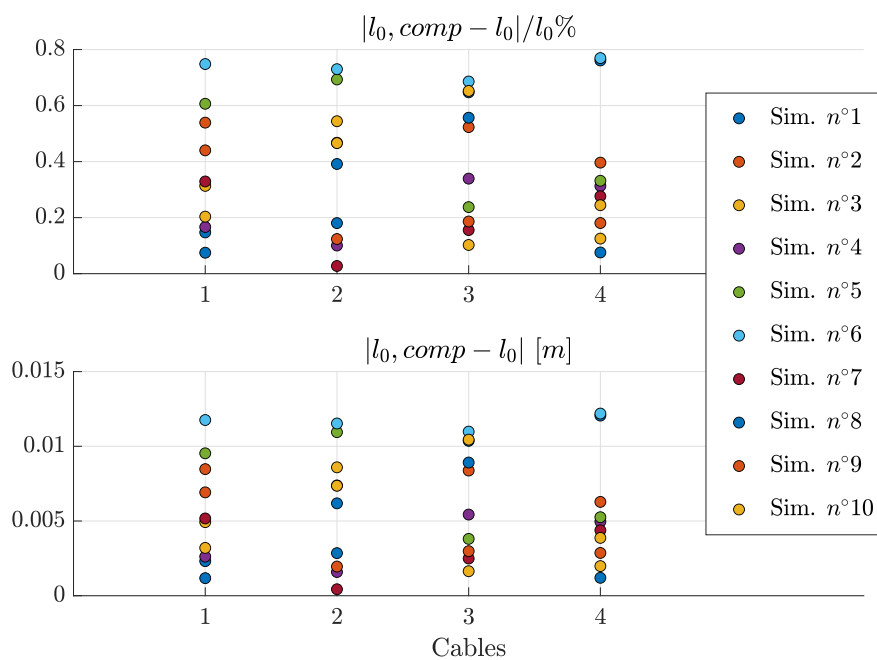


Figure 3.17: Percentage and absolute solution error for measures acquired in Config. C

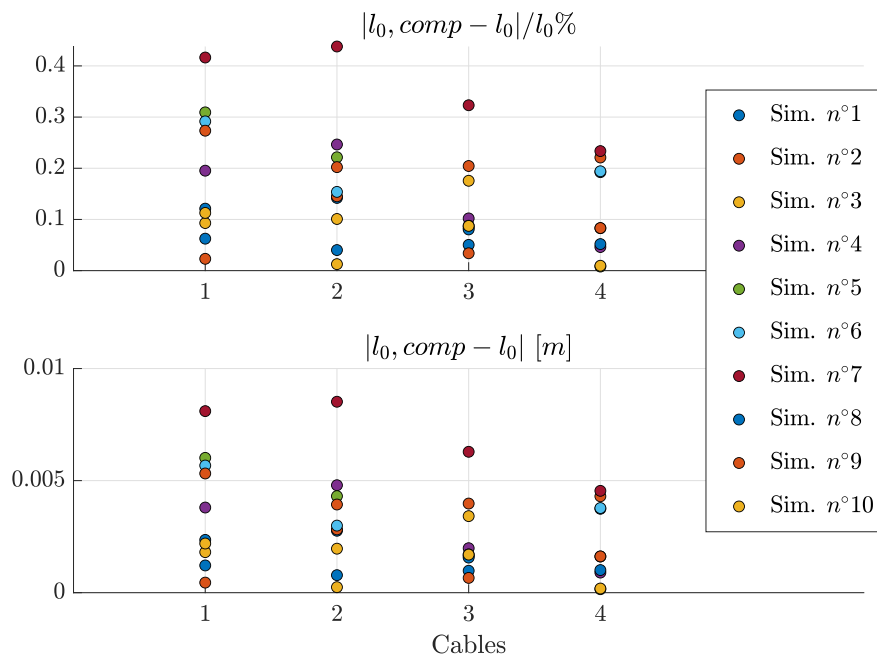


Figure 3.18: Percentage and absolute solution error for measures acquired in Config. D

Chapter 4

Sensitivity indices

Parallel robots and *CDPRs* are, nowadays, used in a larger number of application areas. In the context of control, it is desirable to obtain an estimate of the accuracy of the manipulator, namely to know how errors on actuators affect the displacement of the *EE*. More generally, it is desirable to have a method that allows controlling the impact of errors on measured kinematic variables involved in determining the pose of the *EE*. This issue is central to both serial and parallel robots and has therefore been studied extensively: various accuracy indices have been defined.

In [20] a review of the classical accuracy indices is proposed. First, the *manipulability* accuracy index is introduced. Its purpose is to quantify the manipulator's velocity transmission capabilities. If \mathbf{J} is the Jacobian matrix defining the linear relationship between the time derivative of a joint variable vector and the twist of the *EE*, the manipulability index is calculated as $m = \sqrt{|\mathbf{J}\mathbf{J}^T|}$, where $|\cdot|$ is the matrix norm of (\cdot) . Regardless of the matrix norm chosen, m always represents the amplification between the joint space errors and the generalized coordinate errors. Then the *condition number* index is introduced. Its purpose is to characterize the dexterity of the robot and to express how a relative error in the vector of joint variables is multiplied and results in a relative error in determining the pose of the *EE*.

Although certainly useful in other contexts, these performance indices are not usable for *UACDPRs* because of their inapplicability to dimensionally non-homogeneous Jacobian matrices. In [21], an overview is given of some of the main indices that have been proposed to account for the differences in units between the components of a Jacobian matrix. The approach adopted in this work is to separate the translational and rotational *DoFs* of the *EE*, that is, to use different indices (the maximum rotation and maximum point displacement sensitivity indices) to evaluate the effects of errors on measures on the position and orientation of the platform. There are few studies on the sensitivity of *EE* pose to control or measurement errors. In [22], these indices were computed and compared for revolute-input and prismatic-input Delta robots. A sensitivity analysis was performed in [23] for planar overconstrained *CDPRs* and in [24] for spatially suspended *UACDPRs*. Finally, Ref. [25] evaluated how the pose of a translational *CDPR* changes when some errors of known size are introduced in the cable lengths.

In this Chapter, following the approach described in [21], we investigate both point-displacement and yaw sensitivity to cable-length and roll and pitch errors: sensitivities are obtained through the differential analysis of the robot's geometric constraint equations. We also use these definitions to determine the maximum error of the direct

kinematics solution when the errors on swivel angles, cable lengths, and on pitch and roll angles are within certain bounds.

In Chapter 3, three algorithms are proposed to determine the initial cable lengths of an *UACDPR* and simulations are performed for a 4-cable robot. The simulations show that the results are affected by errors for which an upper bound can be established. In addition, the upper bound for pitch and roll errors is determined by the accuracy of the inclinometers employed. If a method for calculating the maximum point- displacement and yaw errors for given upper bounds on cable- length, pitch and roll errors is determined, it will be possible to compute how inaccuracies in the computation of initial cable lengths would affect the determination of the initial pose for each simulation performed in Chapter 3.

4.1 Kinematic Sensitivity Indices for *UACDPRs*

In this work, sensitivity indices are computed following the approach proposed in [21], namely separating the translational and the rotational *DoFs* of the *EE*. The key idea of this method is to find, among the possible combinations of actuation errors with fixed norm, the two that give global extrema on the norms of the errors on *EE* position and orientation. More generally, it is possible to extend the method and find the combinations of errors on measured kinematic variables with fixed norms that give global extrema on the norms of the errors on parameters to be determined.

An *UACDPR* is characterized by vectors of geometric variables θ that define its configuration in space¹, the knowledge of which allows to compute the *EE* pose ζ (Eqs. 2.10, 2.18, 2.23). Differentiating a loop-closure equation of such a robotic manipulator yields a system of equations of the form:

$$\dot{\theta} = \mathbf{J}\dot{\zeta} \quad (4.1)$$

If $d\theta$ and $d\zeta$ are small errors on measured geometric variables and small errors on the computed pose of the *EE*, holds true:

$$d\theta = \mathbf{J}d\zeta \quad (4.2)$$

In the following chapters, a 6-*DoF EE* suspended by 4 cables equipped with static inclinometers directly measuring pitch-and-roll orientation parameters is considered, so that the problem is well-posed, namely, it comprises a set of 4 nonlinear equations (Eq. 4.2), in 4 unknowns $d\zeta_c$, the errors on computed *EE* position and yaw.

Manipulating Eq. 2.83 yields:

$$d\zeta = \mathbf{P}^T \begin{bmatrix} d\zeta_c \\ d\zeta_f \end{bmatrix} \quad (4.3)$$

also, considerations made in section 2.4 for the Jacobian cable-lengths matrix, are extendable to the Jacobian matrices \mathbf{J}_σ and \mathbf{J}_ψ . In particular, Eq. 2.92 for any Jacobian matrix \mathbf{J} takes the following form:

$$\mathbf{J} = \mathbf{J}_P \mathbf{P} = [\mathbf{J}_c \quad \mathbf{J}_f] \mathbf{P} \quad (4.4)$$

¹For the n -cables *UACDPR* described in Chapter 2, θ represents geometric variables σ , ψ and \mathbf{l}

Substituting in Eq. 4.2 Eqs. 4.3 and 4.4 yields:

$$[\mathbf{J}_c \quad \mathbf{J}_f] \mathbf{P} \mathbf{P}^T \begin{bmatrix} d\zeta_c \\ d\zeta_f \end{bmatrix} = d\boldsymbol{\theta} \quad (4.5)$$

whereas \mathbf{P} is an orthogonal matrix (see Sec. 2.4), hence $\mathbf{P} \mathbf{P}^T = \mathbf{I}_{6 \times 6}$, thus leading to:

$$\mathbf{J}_c d\zeta_c = d\boldsymbol{\theta} - \mathbf{J}_f d\zeta_f \quad (4.6)$$

with $d\zeta_f$ and $d\boldsymbol{\theta}$ representing small errors on acquired measures, and $d\zeta_c$ representing errors on the solution to be determined.

The aim of this Chapter is to define sensitivity indices that describe the sensitivity of the robot position and orientation to errors on acquired measures. Among all computable sensitivity indices proposed in the literature, in order to evaluate the performances of our *UACDPR*, kinematic sensitivity indices have been chosen because of their features:

- the consistency in terms of dimensional units
- the comparability of indices computed for different machines
- the non-dependence of rotational kinematic sensitivity on the choice of the reference point P on the *EE*
- the well-defined physical meaning: a kinematic sensitivity index is the amplification factor between a certain norm of errors on measured geometric variables and the maximum value of a certain norm of errors on the solution.

4.1.1 Sensitivities to errors on measured geometric variables

In order to compute the sensitivities of the unknown parameters ζ_c to errors on measured geometric variables, we assume to have no errors on sensors measuring roll and pitch, that is, $d\zeta_f = \mathbf{0}$:

$$\mathbf{J}_c d\zeta_c = d\boldsymbol{\theta} \quad (4.7)$$

Out of singularities, matrix \mathbf{J}_c is full rank, and thus invertible. If $\mathbf{M} = \mathbf{J}_c^{-1}$, we have:

$$d\zeta_c = \mathbf{M} d\boldsymbol{\theta} \quad (4.8)$$

To compute dimensionally consistent sensitivity indices, it is necessary to decouple unknown pose-parameters: point-position vector \mathbf{p} and yaw angle ψ . Matrix \mathbf{M} can be decoupled in two dimensionally-consistent parts as well, so that Eq. (4.8) becomes:

$$\begin{bmatrix} d\mathbf{p} \\ d\psi \end{bmatrix} = \begin{bmatrix} \mathbf{M}_p \\ \mathbf{M}_\psi \end{bmatrix} d\boldsymbol{\theta} \quad (4.9)$$

or, in another form:

$$d\mathbf{p} = \mathbf{M}_p d\boldsymbol{\theta} \quad (4.10)$$

$$d\psi = \mathbf{M}_\psi d\boldsymbol{\theta} \quad (4.11)$$

where $\mathbf{M}_p \in \mathbb{R}^{3 \times 4}$ and $\mathbf{M}_\psi \in \mathbb{R}^{1 \times 4}$, such that $\mathbf{M} = [\mathbf{M}_p^T \quad \mathbf{M}_\psi^T]^T$.

Finally, we define the *point-displacement kinematic sensitivity to errors on measured geometric variables* as:

$$S_{q,s}^{p,\theta} = \max_{\|\mathbf{d}\boldsymbol{\theta}\|_q=1} \|\mathbf{d}\mathbf{p}\|_s \quad (4.12)$$

where $\|\cdot\|_q$ and $\|\cdot\|_s$ are the q -norm and the s -norm of (\cdot) . According to observations presented in [25], we chose the infinity-norm for $\mathbf{d}\boldsymbol{\theta}$ ($q = \infty$), and the 2-norm for $\mathbf{d}\mathbf{p}$ ($s = 2$), since they attain the clearest physical meaning², thus leading to:

$$S_{\infty,2}^{p,\theta} = \max_{\|\mathbf{d}\boldsymbol{\theta}\|_\infty=1} \|\mathbf{d}\mathbf{p}\|_2 \quad (4.13)$$

Substituting Eq. (4.10) in Eq. (4.13), yields:

$$S_{\infty,2}^{p,\theta} = \max_{\|\mathbf{d}\boldsymbol{\theta}\|_\infty=1} \|\mathbf{M}_p \mathbf{d}\boldsymbol{\theta}\|_2 \quad (4.14)$$

that is, by definition [25], the matrix \mathbf{M}_p norm induced by $\|\cdot\|_2$ and $\|\cdot\|_\infty$:

$$S_{\infty,2}^{p,\theta} = \|\mathbf{M}_p\|_{\infty,2} \quad (4.15)$$

The computation of the norm of a matrix-induced by $\|\cdot\|_2$ and $\|\cdot\|_\infty$ is, in terms of computational complexity, NP-hard, namely, no known algorithm can do so in polynomial time [26], still is preferable to computing the solution of the generally nonlinear convex optimization problem 4.13.

Similarly, *yaw sensitivity to errors on measured geometric variables* can be defined as:

$$S_{\infty,2}^{\psi,\theta} = \max_{\|\mathbf{d}\boldsymbol{\theta}\|_\infty=1} \|\mathbf{d}\psi\|_2 \quad (4.16)$$

Substituting Eq. 4.11 therein, we show that yaw angle sensitivity is equal to the matrix \mathbf{M}_ψ norm induced by $\|\cdot\|_2$ and $\|\cdot\|_\infty$, namely:

$$S_{\infty,2}^{\psi,\theta} = \|\mathbf{M}_\psi\|_{\infty,2} \quad (4.17)$$

4.1.2 Sensitivities to Errors on Roll and Pitch Measurements

In order to compute ζ_c sensitivity to errors on roll and pitch measurements we assume $\mathbf{d}\boldsymbol{\theta} = \mathbf{0}$; Eq. (4.6) thus becomes:

$$\mathbf{J}_c \mathbf{d}\zeta_c = -\mathbf{J}_f \mathbf{d}\zeta_f \quad (4.18)$$

Out of singularities, matrix \mathbf{J}_c is full rank, and thus invertible. We have:

$$\mathbf{d}\zeta_c = \mathbf{N} \mathbf{d}\zeta_f \quad (4.19)$$

where $\mathbf{N} = -\mathbf{J}_c^{-1} \mathbf{J}_f \in \mathbb{R}^{4 \times 2}$. Matrix \mathbf{N} can be decoupled in two dimensionally-consistent parts so that Eq. (4.19) becomes:

$$\begin{bmatrix} \mathbf{d}\mathbf{p} \\ \mathbf{d}\psi \end{bmatrix} = \begin{bmatrix} \mathbf{N}_p \\ \mathbf{N}_\psi \end{bmatrix} \mathbf{d}\zeta_f \quad (4.20)$$

²The norm $\|\mathbf{d}\boldsymbol{\theta}\|_\infty = 1$, states that the absolute value of the measurements errors are independently bound by 1, while the 2-norm $\|\mathbf{d}\mathbf{p}\|_2$ indicates the maximum distance error.

or, in another form:

$$d\mathbf{p} = \mathbf{N}_p d\boldsymbol{\zeta}_f \quad (4.21)$$

$$d\psi = \mathbf{N}_\psi d\boldsymbol{\zeta}_f \quad (4.22)$$

where $\mathbf{N}_p \in \mathbb{R}^{3 \times 2}$ and $\mathbf{N}_\psi \in \mathbb{R}^{1 \times 2}$ such that matrix $\mathbf{N} = [\mathbf{N}_p^T \quad \mathbf{N}_\psi^T]^T$.

It is now possible to define the *point-displacement sensitivity to errors in roll-and-pitch measurements* as:

$$S_{\infty,2}^{p,\zeta_f} = \max_{\|d\boldsymbol{\zeta}_k\|_\infty=1} \|d\mathbf{p}\|_2 \quad (4.23)$$

then, substituting Eq. (4.21) therein, we obtain the matrix \mathbf{N}_p norm induced by $\|\cdot\|_2$ and $\|\cdot\|_\infty$:

$$S_{\infty,2}^{p,\zeta_f} = \|\mathbf{N}_p\|_{\infty,2} \quad (4.24)$$

Similarly, we define the *yaw sensitivity to errors in roll-and-pitch measurements* as:

$$S_{\infty,2}^{\psi,\zeta_f} = \max_{\|d\boldsymbol{\zeta}_k\|_\infty=1} \|d\psi\|_2 \quad (4.25)$$

and substituting Eq. (4.20) therein, we obtain the matrix \mathbf{N}_ψ norm induced by $\|\cdot\|_2$ and $\|\cdot\|_\infty$:

$$S_{\infty,2}^{\psi,\zeta_f} = \|\mathbf{N}_\psi\|_{\infty,2} \quad (4.26)$$

4.1.3 Maximum combined point-displacement and yaw errors

Kinematic sensitivity indices computed as indicated have a well-defined physical meaning. From Eqs. 4.13, 4.16 we can get the module of the maximum distance between the real and the computed position of the *EE*, namely the maximum error committed in determining the *EE* position, and the absolute value of the maximum difference between the real and the computed yaw orientation angle, namely the maximum error committed in determining the *EE* yaw angle, if the infinity norm of the errors on measured geometric variables $d\boldsymbol{\theta}$, namely the maximum committable error in measuring those variables, is known:

$$\|d\mathbf{p}_{max}\|_2 = S_{\infty,2}^{p,\theta} \|d\boldsymbol{\theta}\|_\infty \quad (4.27)$$

$$\|d\psi_{max}\|_2 = S_{\infty,2}^{\psi,\theta} \|d\boldsymbol{\theta}\|_\infty \quad (4.28)$$

Similarly, from Eqs. 4.23, 4.25 we can get the modules of maximum errors committed in determining the *EE* position and yaw orientation angle, for a known maximum committable error in measuring roll and pitch angles:

$$\|d\mathbf{p}_{max}\|_2 = S_{\infty,2}^{p,\zeta_f} \|d\boldsymbol{\zeta}_f\|_\infty \quad (4.29)$$

$$\|d\psi_{max}\|_2 = S_{\infty,2}^{\psi,\zeta_f} \|d\boldsymbol{\zeta}_f\|_\infty \quad (4.30)$$

If the infinity norm of the errors on measured geometric variables $d\boldsymbol{\theta}_{max} = \|d\boldsymbol{\theta}\|_\infty$ and roll-and-pitch angles $d\boldsymbol{\zeta}_{f,max} = \|d\boldsymbol{\zeta}_f\|_\infty$ are known, the computed sensitivity indices can be employed to evaluate the maximum combined point-displacement and yaw errors:

$$\|d\mathbf{p}_{max}\|_2 = S_{\infty,2}^{p,\theta} d\boldsymbol{\theta}_{max} + S_{\infty,2}^{p,\zeta_f} d\boldsymbol{\zeta}_{f,max} \quad (4.31)$$

$$\|d\psi_{max}\|_2 = S_{\infty,2}^{\psi,\theta} d\boldsymbol{\theta}_{max} + S_{\infty,2}^{\psi,\zeta_f} d\boldsymbol{\zeta}_{f,max} \quad (4.32)$$

4.2 Sensitivity to Errors in Cable Lengths and Pitch and Roll Angles

In this Section, the theoretical point-displacement and yaw sensitivities to cable-length, roll and pitch errors are introduced. A 6-DoF EE suspended by 4 cables is considered, so that the direct kinematics with cable lengths, roll and pitch measurements is well-posed, namely, it comprises a set of 4 nonlinear equations, the geometrical constraints in Eq. (2.23), in 4 unknowns ζ_c , the EE position and yaw.

4.2.1 Sensitivity Indices

In this Section the measured geometric variables are cable lengths \mathbf{l} , thus, the first-order differential equation considered is Eq. 2.53, and the Jacobian matrix considered is the cable length Jacobian matrix \mathbf{J}_l . If $d\mathbf{l}$ and $d\zeta_f$ are small errors on the measures of cable lengths and pitch and roll angles, and $d\zeta_c$ are small errors on the solution to be determined, Eq. 4.6 becomes:

$$\mathbf{J}_{l,c}d\zeta_c = d\mathbf{l} - \mathbf{J}_{l,f}d\zeta_f \quad (4.33)$$

By assuming, firstly, to have no errors on sensors measuring roll and pitch, following the approach described in Section 4.1, we can define the *point-displacement kinematic sensitivity to errors in cable-length measurements*:

$$S_{\infty,2}^{p,l} = \max_{\|d\mathbf{l}\|_{\infty}=1} \|d\mathbf{p}\|_2 \quad (4.34)$$

and *yaw sensitivity to errors in cable-length measurements*

$$S_{\infty,2}^{\psi,l} = \max_{\|d\mathbf{l}\|_{\infty}=1} \|d\psi\|_2 \quad (4.35)$$

If matrix $\mathbf{M}_l = \mathbf{J}_{l,c}^{-1}$, and $\mathbf{M}_{l,p} \in \mathbb{R}^{3 \times 4}$ and $\mathbf{M}_{l,\psi} \in \mathbb{R}^{1 \times 4}$, such that $\mathbf{M}_l = [\mathbf{M}_{l,p}^T \quad \mathbf{M}_{l,\psi}^T]^T$:

$$d\mathbf{p} = \mathbf{M}_{l,p}d\mathbf{l} \quad (4.36)$$

$$d\psi = \mathbf{M}_{l,\psi}d\mathbf{l} \quad (4.37)$$

and the sensitivity indices in Eqs. 4.34, 4.35 are equal to matrices $\mathbf{M}_{l,p}$ $\mathbf{M}_{l,\psi}$ norms induced by $\|\cdot\|_2$ and $\|\cdot\|_{\infty}$:

$$S_{\infty,2}^{p,l} = \|\mathbf{M}_{l,p}\|_{\infty,2} \quad (4.38)$$

$$S_{\infty,2}^{\psi,l} = \|\mathbf{M}_{l,\psi}\|_{\infty,2} \quad (4.39)$$

Secondly, by assuming to have no errors on sensors measuring cable lengths, that is $d\mathbf{l} = \mathbf{0}$, we can define the *point-displacement kinematic sensitivity to errors in roll-and-pitch measurements*:

$$S_{\infty,2}^{p,\zeta_f} = \max_{\|d\zeta_f\|_{\infty}=1} \|d\mathbf{p}\|_2 \quad (4.40)$$

and the *yaw sensitivity to errors in roll-and-pitch measurements*:

$$S_{\infty,2}^{\psi,\zeta_f} = \max_{\|d\zeta_f\|_{\infty}=1} \|d\psi\|_2 \quad (4.41)$$

If matrix $\mathbf{N}_l = -\mathbf{J}_{l,c}^{-1}\mathbf{J}_{l,f}$, and $\mathbf{N}_{l,p} \in \mathbb{R}^{3 \times 2}$ and $\mathbf{N}_{l,\psi} \in \mathbb{R}^{1 \times 2}$ such that $\mathbf{N}_l = [\mathbf{N}_{l,p}^T \quad \mathbf{N}_{l,\psi}^T]^T$:

$$d\mathbf{p} = \mathbf{N}_{l,p} d\zeta_f \quad (4.42)$$

$$d\psi = \mathbf{N}_{l,\psi} d\zeta_f \quad (4.43)$$

the sensitivity index in Eqs. 4.40, 4.41 are equal to matrices $\mathbf{N}_{l,p}$, $\mathbf{N}_{l,\psi}$ norms induced by $\|\cdot\|_2$ and $\|\cdot\|_\infty$:

$$S_{\infty,2}^{p,\zeta_f} = \|\mathbf{N}_{l,p}\|_{\infty,2} \quad (4.44)$$

$$S_{\infty,2}^{\psi,\zeta_f} = \|\mathbf{N}_{l,\psi}\|_{\infty,2} \quad (4.45)$$

In addition, if maximum errors committed in measuring cable lengths dl_{max} and roll-and-pitch angles $d\zeta_{f,max}$ are known, the aforementioned sensitivity indices can be employed to evaluate the maximum combined point-displacement and yaw errors (see Subsec. 4.1.3):

$$\|d\mathbf{p}_{max}\|_2 = S_{\infty,2}^{p,l} dl_{max} + S_{\infty,2}^{p,\zeta_f} d\zeta_{f,max} \quad (4.46)$$

$$\|d\psi_{max}\|_2 = S_{\infty,2}^{\psi,l} dl_{max} + S_{\infty,2}^{\psi,\zeta_f} d\zeta_{f,max} \quad (4.47)$$

4.2.2 Simulation Results

In this section, we present the application of the proposed sensitivity indices throughout the static workspace [27] of a 4-cable *UACDPR* whose platform mass is $m = 1\text{kg}$ and whose geometrical properties are summarized in Tables 3.1, 3.2. Point-displacement and yaw sensitivities to errors in cable-length measurements are computed according to Eqs. (4.38), (4.39); the matrix norms induced by $\|\cdot\|_2$ and $\|\cdot\|_\infty$ are calculated by way of the algorithm proposed in [28].

In the given workspace, the results range from 1.78 to 6.19 mm/mm for $S_{\infty,2}^{p,l}$, and from 0.77 to 1.51 °/mm for $S_{\infty,2}^{\psi,l}$. The position vector \mathbf{p} is more sensitive to errors in cable lengths in the upper central part of the workspace, whereas the yaw orientation angle ψ is more sensitive to errors in cable lengths in the lower side parts (Fig. 4.1).

Point-displacement and yaw sensitivities to errors in roll-and-pitch measurements are computed according to Eqs. (4.44), (4.45); in the given workspace, the results range from 0.64 to 3.89 mm/° for $S_{\infty,2}^{p,\zeta_f}$, and from 0.01 to 1.81 °/° for $S_{\infty,2}^{\psi,\zeta_f}$. \mathbf{p} is more sensitive to errors in pitch and roll in the lower and upper parts of the workspace, whereas ψ is more sensitive to errors in pitch and roll in the lateral parts (Fig. 4.2). In addition, if maximum errors in cable lengths dl_{max} and in roll-and-pitch angles $d\zeta_{f,max}$ are known, the aforementioned sensitivity indices can be employed to evaluate the maximum combined point-displacement and yaw errors (Eqs. 4.46 4.47).

The simulations performed in Subsec. 3.1.2 shows that, even if measures are acquired exciting the platform in 11 different points in the workspace (Config. *D*, Fig. 3.9), the absolute maximum error in the determination of the initial cable lengths is 20mm. Thus, assuming $dl_{max} = 20\text{mm}$ and $d\zeta_{f,max} = 0.2^\circ$, the accuracy on the determination of *EE* position and yaw orientation angle can be computed throughout the workspace, showing how errors in cable lengths computation would affect the determination of the initial pose. In the center of the workspace, the accuracy in the determination of the *EE* position \mathbf{p} is around 40mm, while the accuracy in the determination of the yaw angle ψ is around 15° (Fig. 4.3).

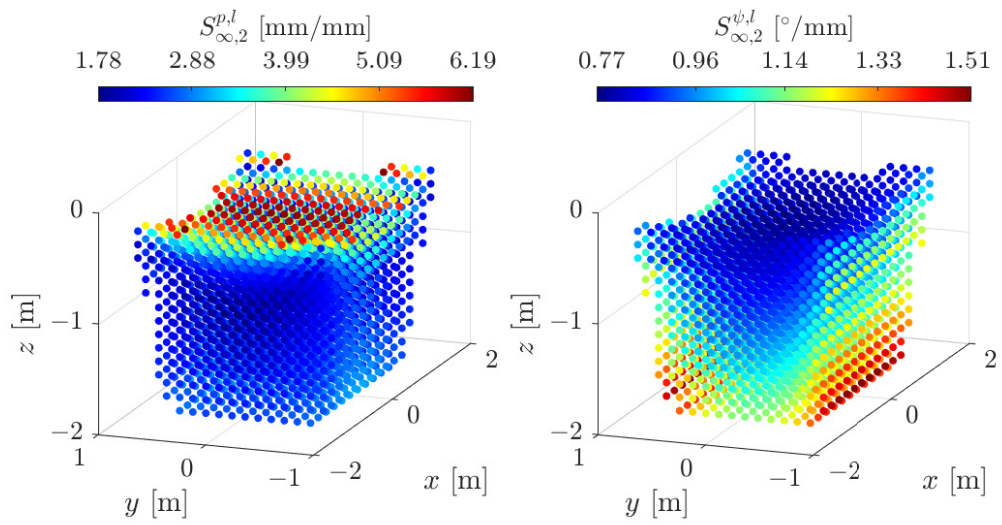


Figure 4.1: Point-displacement and yaw sensitivities to errors in cable-length measurements

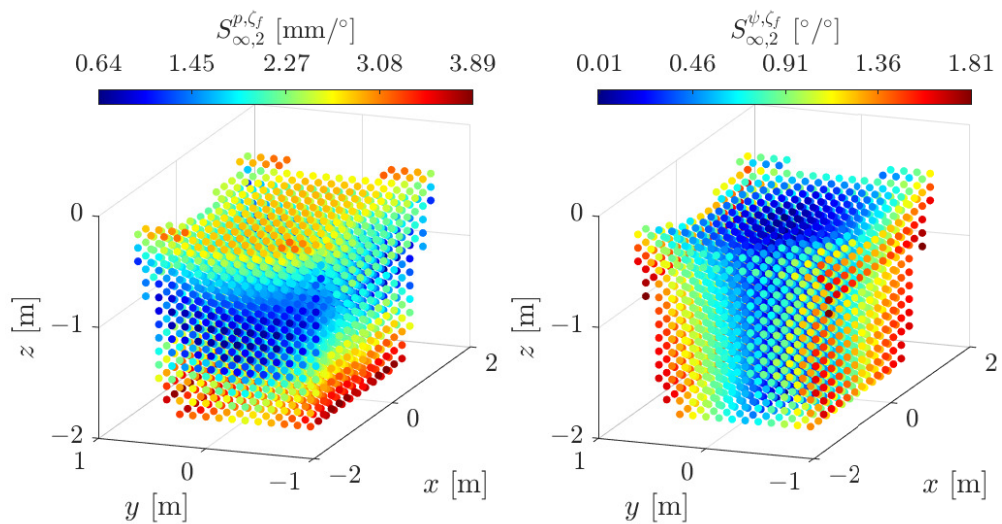


Figure 4.2: Point-displacement and yaw sensitivities to errors in roll-and-pitch measurements

Higher accuracies are obtained, for both \mathbf{p} and ψ , considering results obtained from simulations performed in Subsec. 3.3.2. If measures are acquired exciting the platform in 6 different points in the workspace (Config C, Fig. 3.7), and the *EE* is equipped with inclinometers measuring roll-and-pitch angles, the absolute maximum error in the determination of the initial cable lengths is 15mm. Thus, assuming $dl_{max} = 15\text{mm}$ and $d\zeta_{f,max} = 0.2^\circ$, the accuracy on the determination of *EE* position and yaw orientation angle can be computed throughout the workspace. In the center of the workspace, the accuracy in the determination of the *EE* position \mathbf{p} is around 30mm, while the accuracy in the determination of the yaw angle ψ is around 12° (Fig. 4.4). If measures are acquired exciting the platform in 11 different points in the workspace (Config D, Fig. 3.9), the absolute maximum error in the determination of the initial cable lengths is 10mm. Thus, assuming $dl_{max} = 10\text{mm}$ and $d\zeta_{f,max} = 0.2^\circ$, the accuracy on the determination of *EE* position and yaw orientation angle can be computed throughout the workspace. In the center of the workspace, the accuracy in the determination of the *EE* position \mathbf{p} is around 20mm, while the accuracy in the determination of the yaw angle ψ is around 8° (Fig. 4.3).

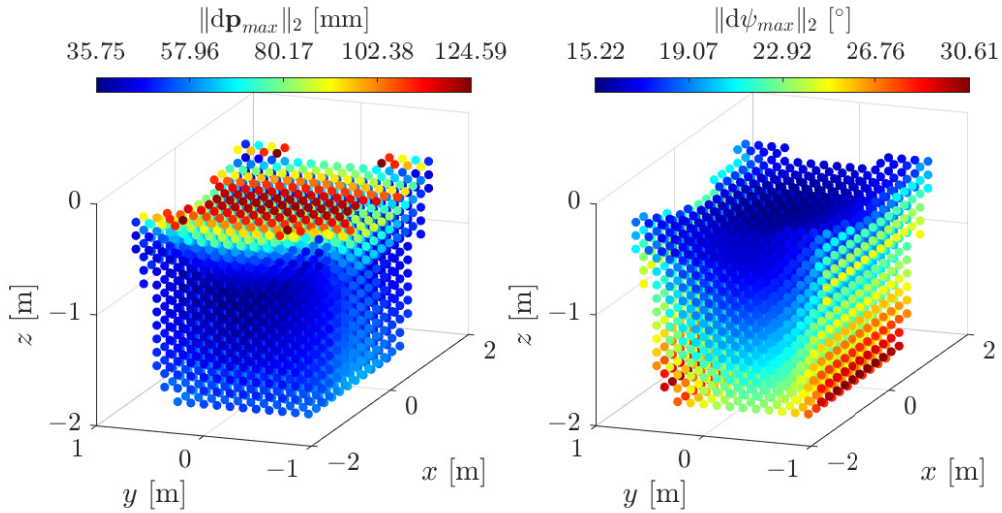


Figure 4.3: Point-displacement and yaw accuracies for $dl_{max} = 20$ mm and $d\zeta_{f,max} = 0.2^\circ$

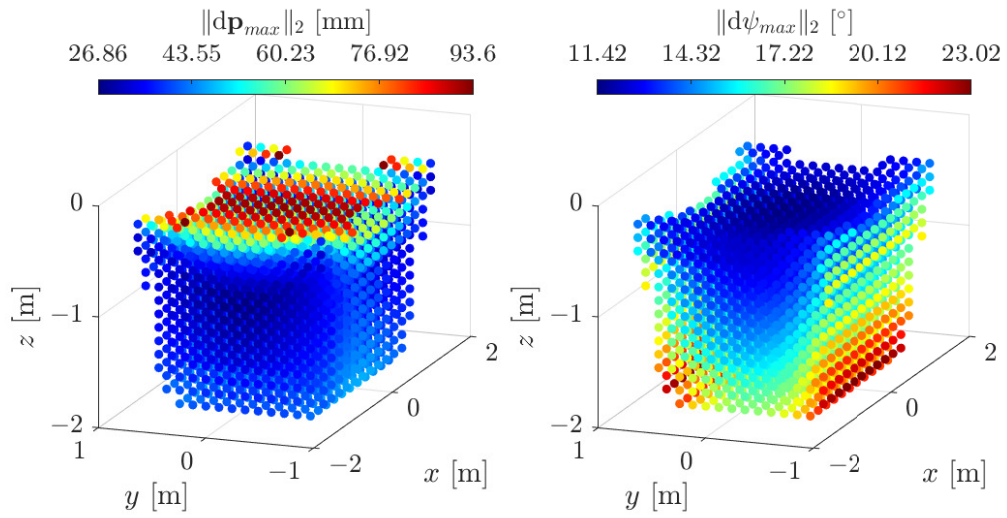


Figure 4.4: Point-displacement and yaw accuracies for $d l_{max} = 15$ mm and $d\check{\zeta}_{f,max} = 0.2^\circ$

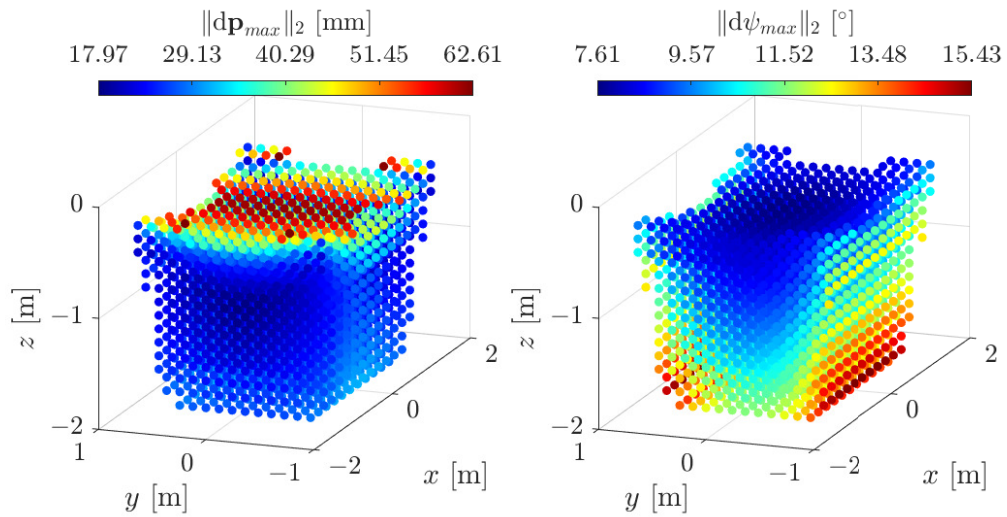


Figure 4.5: Point-displacement and yaw accuracies for $d l_{max} = 10$ mm and $d\check{\zeta}_{f,max} = 0.2^\circ$

4.3 Sensitivity to Errors in Swivel Angles and Pitch and Roll Angles

The aim of this Section is to compute the theoretical point-displacement and yaw sensitivities to swivel angles, roll and pitch errors. A 6-DoF EE suspended by 4 cables is considered, so that the direct kinematics with swivel angles, roll and pitch measurements is well-posed, namely, it comprises a set of 4 nonlinear equations, the geometrical constraints in Eq. (2.10), in 4 unknowns ζ_c , the EE position and yaw.

4.3.1 Sensitivity Indices

In Section 4.1 the concept of sensitivity of the unknowns to the measure of any geometric variables θ was theoretically introduced. In this Section the measured geometric variables are the swivel angles σ , thus, the first-order differential equation considered is Eq. 2.51, and the Jacobian matrix considered is the swivel angle Jacobian matrix \mathbf{J}_σ . If $d\sigma$ and $d\zeta_f$ are small errors on the measures of swivel angles and pitch and roll angles, and $d\zeta_c$ are small errors on the solution to be determined, Eq. 4.6 becomes:

$$\mathbf{J}_{\sigma,c} d\zeta_c = d\sigma - \mathbf{J}_{\sigma,f} d\zeta_f \quad (4.48)$$

By assuming, firstly, to have no errors on sensors measuring roll and pitch, following the approach described in Section 4.1, we can define the *point-displacement kinematic sensitivity to errors in swivel-angle measurements*:

$$S_{\infty,2}^{p,\sigma} = \max_{\|d\sigma\|_\infty=1} \|d\mathbf{p}\|_2 \quad (4.49)$$

and *yaw sensitivity to errors in swivel-angle measurements*

$$S_{\infty,2}^{\psi,\sigma} = \max_{\|d\sigma\|_\infty=1} \|d\psi\|_2 \quad (4.50)$$

If matrix $\mathbf{M}_\sigma = \mathbf{J}_{\sigma,c}^{-1}$, and $\mathbf{M}_{\sigma,p} \in \mathbb{R}^{3 \times 4}$ and $\mathbf{M}_{\sigma,\psi} \in \mathbb{R}^{1 \times 4}$, such that $\mathbf{M}_\sigma = [\mathbf{M}_{\sigma,p}^T \quad \mathbf{M}_{\sigma,\psi}^T]^T$:

$$d\mathbf{p} = \mathbf{M}_{\sigma,p} d\sigma \quad (4.51)$$

$$d\psi = \mathbf{M}_{\sigma,\psi} d\sigma \quad (4.52)$$

the sensitivity index in Eqs. 4.49, 4.50 are equal to matrices $\mathbf{M}_{\sigma,p}$ $\mathbf{M}_{\sigma,\psi}$ norms induced by $\|\cdot\|_2$ and $\|\cdot\|_\infty$:

$$S_{\infty,2}^{p,\sigma} = \|\mathbf{M}_{\sigma,p}\|_{\infty,2} \quad (4.53)$$

$$S_{\infty,2}^{\psi,\sigma} = \|\mathbf{M}_{\sigma,\psi}\|_{\infty,2} \quad (4.54)$$

Secondly, by assuming to have no errors on sensors measuring swivel angles, that is $d\sigma = \mathbf{0}$, we can define the *point-displacement kinematic sensitivity to errors in roll-and-pitch measurements*:

$$S_{\infty,2}^{p,\zeta_f} = \max_{\|d\zeta_f\|_\infty=1} \|d\mathbf{p}\|_2 \quad (4.55)$$

and the *yaw sensitivity to errors in roll-and-pitch measurements*:

$$S_{\infty,2}^{\psi,\zeta_f} = \max_{\|d\zeta_f\|_\infty=1} \|d\psi\|_2 \quad (4.56)$$

If matrix $\mathbf{N}_\sigma = -\mathbf{J}_{\sigma,c}^{-1}\mathbf{J}_{\sigma,f}$, and $\mathbf{N}_{\sigma,p} \in \mathbb{R}^{3 \times 2}$ and $\mathbf{N}_{\sigma,\psi} \in \mathbb{R}^{1 \times 2}$ such that $\mathbf{N}_\sigma = [\mathbf{N}_{\sigma,p}^T \quad \mathbf{N}_{\sigma,\psi}^T]^T$:

$$d\mathbf{p} = \mathbf{N}_{\sigma,p} d\check{\zeta}_f \quad (4.57)$$

$$d\psi = \mathbf{N}_{\sigma,\psi} d\check{\zeta}_f \quad (4.58)$$

the sensitivity indices in Eqs. 4.55, 4.56 are equal to matrices $\mathbf{N}_{\sigma,p}$, $\mathbf{N}_{\sigma,\psi}$ norms induced by $\|\cdot\|_2$ and $\|\cdot\|_\infty$:

$$S_{\infty,2}^{p,\zeta_f} = \|\mathbf{N}_{\sigma,p}\|_{\infty,2} \quad (4.59)$$

$$S_{\infty,2}^{\psi,\zeta_f} = \|\mathbf{N}_{\sigma,\psi}\|_{\infty,2} \quad (4.60)$$

In addition, if maximum errors committed in measuring swivel angles $d\sigma_{max}$ and roll-and-pitch angles $d\check{\zeta}_{f,max}$ are known, the aforementioned sensitivity indices can be employed to evaluate the maximum combined point-displacement and yaw errors (see Subsec. 4.1.3):

$$\|d\mathbf{p}_{max}\|_2 = S_{\infty,2}^{p,\sigma} d\sigma_{max} + S_{\infty,2}^{p,\zeta_f} d\check{\zeta}_{f,max} \quad (4.61)$$

$$\|d\psi_{max}\|_2 = S_{\infty,2}^{\psi,\sigma} d\sigma_{max} + S_{\infty,2}^{\psi,\zeta_f} d\check{\zeta}_{f,max} \quad (4.62)$$

Chapter 5

Conclusions

5.1 Main Results

In this thesis, the problem of determining the initial lengths of cables when an *UACDPR* is in a start-up condition was tackled. An analytical formulation of a possible solution algorithm was developed and an initial position calibration procedure that measures swivel angles and roll-and-pitch angles when the platform is in *free motion* was proposed. The solution of this problem is critical in particular for *UACDPRs* equipped with incremental encoders measuring cable lengths: for these robots, the initial cable lengths are parameters that must be determined at power-up to be used to calculate subsequent *EE* poses as the robot moves to perform tasks. Simulations performed on MATLAB® on a 6-*DoF EE* suspended by 4 cables proved to be unsatisfactory. The minimum percentage error in determining the cable lengths is 0.5%

However, the need to evaluate how errors in the determination of initial cable lengths affect the determination of the *EE* pose has led to the development of a computationally efficient method for calculating kinematic sensitivity indices for the rotational and translational *DoFs* of the *EE*. It has been shown that these indices can be used to determine the maximum errors committed in determining the *EE* pose. They can also be used to compare the accuracy of different manipulators.

5.2 Open Issues

In order to improve the accuracy of the calibration algorithm, the use of different types of proprioceptive sensors or the measurement of different pose parameters or other model variables could be explored. Also, the proposed algorithms could be modified to account for both kinematics and dynamics equations. However, the feasibility of such a procedure needs to be evaluated because dynamic models are often simplified and may not be suitable for calibration purposes. Furthermore, a sensitivity analysis can be performed to evaluate how errors in measured swivel angles or other acquired data sets affect the results of the algorithm.

Appendices

Appendix A

Backward finite difference method

This appendix presents the finite difference method, a technique used in this thesis in order to approximate the free pose-coordinates first-order derivative to an arbitrary order of accuracy.

In general, the Taylor polynomial of function $\zeta(t)$ at point t_k is:

$$\zeta(t) = \sum_{n=0}^N \frac{\zeta^{(n)}(t_k)}{n!} (t - t_k)^n + o(|t - t_k|^N) \quad (\text{A.1})$$

where superscript $^{(n)}$ indicates the $n - th$ order time derivative of function $\zeta(t)$. If the uniform grid time spacing is sufficiently thin, specifically if $h = |t - t_k|$ is sufficiently small, this polynomial could be used as an approximation of $\zeta(t)$ for t near the point t_k .

If we choose a particular set of $N + 1$ points in the temporal domain:

$$[t_k - Nh, \dots, t_k - jh, \dots, t_k - h, t_k] = [t_{k-N}, \dots, t_{k-j}, \dots, t_{k-1}, t_k] \quad (\text{A.2})$$

Taylor polynomials of functions $\zeta(t_{k-j})$ at points t_k can be written as:

$$\zeta(t_{k-j}) = \sum_{n=0}^N \frac{\zeta^{(n)}(t_k)}{n!} (t_{k-j} - t_k)^n + o(|t_{k-j} - t_k|^N) \quad \text{for } j = 0, 1, \dots, N \quad (\text{A.3})$$

also, substituting $t_{k-j} - t_k = -jh$ into Eq. (A.3) yields:

$$\zeta(t_{k-j}) = \sum_{n=0}^N \frac{\zeta^{(n)}(t_k)}{n!} (-jh)^n + o(h)^N \quad (\text{A.4})$$

Then, expanding the summation:

$$\zeta(t_{k-j}) = \zeta(t_k) - \zeta'(t_k)(jh) + \frac{\zeta''(t_k)}{2}(jh)^2 - \frac{\zeta'''(t_k)}{6}(jh)^3 + \dots + \frac{\zeta^{(N)}(t_k)}{N!}(-jh)^N + o(h)^N \quad (\text{A.5})$$

and making terms indicated by the subscript j explicit, yields the system of equations:

$$\left\{ \begin{array}{l} \zeta(t_k) = \zeta(t_k) \\ \zeta(t_{k-1}) = \zeta(t_k) - \zeta'(t_k)(h) + \frac{\zeta''(t_k)}{2}(h)^2 - \frac{\zeta'''(t_k)}{6}(h)^3 + \dots + \frac{\zeta^{(N)}(t_k)}{N!}(-h)^N + o(h)^N \\ \zeta(t_{k-2}) = \zeta(t_k) - \zeta'(t_k)(2h) + \frac{\zeta''(t_k)}{2}(2h)^2 - \frac{\zeta'''(t_k)}{6}(2h)^3 + \dots + \frac{\zeta^{(N)}(t_k)}{N!}(-2h)^N + o(h)^N \\ \dots \\ \zeta(t_{k-N}) = \zeta(t_k) - \zeta'(t_k)(Nh) + \frac{\zeta''(t_k)}{2}(Nh)^2 - \frac{\zeta'''(t_k)}{6}(Nh)^3 + \dots + \frac{\zeta^{(N)}(t_k)}{N!}(-Nh)^N + o(h)^N \end{array} \right. \quad (\text{A.6})$$

Finally, we multiply each equation by a coefficient c_j :

$$\begin{cases} c_0 \zeta(t_k) = c_0 \zeta(t_k) \\ c_1 \zeta(t_{k-1}) = c_1 \zeta(t_k) - c_1 \zeta'(t_k)(h) + c_1 \frac{\zeta''(t_k)}{2}(h)^2 + \dots + c_1 \frac{\zeta^{(N)}(t_k)}{N!}(-h)^N + o(h)^N \\ c_2 \zeta(t_{k-2}) = c_2 \zeta(t_k) - c_2 \zeta'(t_k)(2h) + c_2 \frac{\zeta''(t_k)}{2}(2h)^2 + \dots + c_2 \frac{\zeta^{(N)}(t_k)}{N!}(-2h)^N + o(h)^N \\ \dots \\ c_N \zeta(t_{k-N}) = c_N \zeta(t_k) - c_N \zeta'(t_k)(Nh) + c_N \frac{\zeta''(t_k)}{2}(Nh)^2 + \dots + c_N \frac{\zeta^{(N)}(t_k)}{N!}(-Nh)^N + o(h)^N \end{cases} \quad (\text{A.7})$$

and we define a specific set of constraint for coefficients c_j :

$$\begin{cases} \sum_{j=0}^N c_j = 0 \\ \sum_{j=0}^N j c_j = 1 \\ \sum_{j=0}^N j^2 c_j = 0 \\ \dots \\ \sum_{j=0}^N j^N c_j = 0 \end{cases} \quad (\text{A.8})$$

which can be rewritten in matrix form as:

$$\begin{bmatrix} 1 & 1 & 1 & \dots & 1 \\ 0 & 1 & 2 & \dots & N \\ 0^2 & 1^2 & 2^2 & \dots & N^2 \\ \dots & \dots & \dots & \dots & \dots \\ 0^N & 1^N & 2^N & \dots & N^N \end{bmatrix} \begin{bmatrix} c_0 \\ c_1 \\ c_2 \\ \dots \\ c_N \end{bmatrix} = \begin{bmatrix} 0 \\ 1 \\ 0 \\ \dots \\ 0 \end{bmatrix} \quad (\text{A.9})$$

This particular set of constraints allow us to extrapolate an approximation of vector $\zeta'(t_k)$. Indeed, the sum of the equations of the system (A.7), rearranging and simplifying terms, yields:

$$\zeta'(t_k) = \frac{c_0 \zeta(t_k) + c_1 \zeta(t_{k-1}) + c_2 \zeta(t_{k-2}) + \dots + c_N \zeta(t_{k-N})}{h} + o(h)^N \quad (\text{A.10})$$

where coefficients c_j can be obtained by the solution of system (A.9).

Regrouping the $N+1$ poses ζ_j in a $6 \times (N+1)$ matrix \mathbf{Z}_k :

$$\mathbf{Z}_k = [\zeta(t_{k-N}), \zeta(t_{k-N+1}), \dots, \zeta(t_k)] = [\zeta_{k-N}, \zeta_{k-N+1}, \dots, \zeta_k] \quad (\text{A.11})$$

and the $N+1$ coefficients c_j in a $(N+1) \times 1$ vector \mathbf{C} :

$$\mathbf{C} = \begin{bmatrix} c_1 \\ c_2 \\ \vdots \\ c_N \end{bmatrix} \quad (\text{A.12})$$

equation A.10 can be approximated as:

$$\zeta'(t_k) \simeq \frac{1}{h} \mathbf{Z}_k \mathbf{C} \quad (\text{A.13})$$

It should be noted that the order of accuracy of the approximation is $o(h)^N$, and thus, hypothetically, increasing the number of points N the approximation can be made as accurate as one likes.

List of Figures

1.1	Collector of the Arecibo Observatory. By H. Schweiker/WIYN and NOAO/AURA/NSF - https://www.flickr.com/photos/nasablueshift/8288406364/ , CC BY 4.0, https://commons.wikimedia.org/w/index.php?curid=113226349	11
1.2	Cable robot used to position TV broadcast cameras, by Despeaux - Own work, CC BY-SA 3.0, https://commons.wikimedia.org/w/index.php?curid=7852833	12
2.1	<i>CDPR</i> Geometric Model	16
2.2	Swivel Pulley Geometric Model	16
2.3	Geometric interpretation of Eq. (2.17) double solution	18
3.1	Config. P_0	31
3.2	Percentage and absolute solution error for measures acquired in Config. P_0	31
3.3	Config. A	32
3.4	Percentage and absolute solution error for measures acquired in Config. A	32
3.5	Config. B	33
3.6	Percentage and absolute solution error for measures acquired in Config. B	33
3.7	Config. C	34
3.8	Percentage and absolute solution error for measures acquired in Config. C	34
3.9	Config. D	35
3.10	Percentage and absolute solution error for measures acquired in Config. D	35
3.11	Percentage and absolute solution error for measures acquired in Config. P_0	38
3.12	Percentage and absolute solution error for measures acquired in Config. A	38
3.13	Percentage and absolute solution error for measures acquired in Config. C	39
3.14	Percentage and absolute solution error for measures acquired in Config. D	39
3.15	Percentage and absolute solution error for measures acquired in Config. P_0	43
3.16	Percentage and absolute solution error for measures acquired in Config. A	43
3.17	Percentage and absolute solution error for measures acquired in Config. C	44
3.18	Percentage and absolute solution error for measures acquired in Config. D	44
4.1	Point-displacement and yaw sensitivities to errors in cable-length measurements	54
4.2	Point-displacement and yaw sensitivities to errors in roll-and-pitch measurements	54
4.3	Point-displacement and yaw accuracies for $dl_{max} = 20$ mm and $d\zeta_{f,max} = 0.2^\circ$	55

4.4	Point-displacement and yaw accuracies for $dl_{max} = 15$ mm and $d\zeta_{f,max} = 0.2^\circ$	56
4.5	Point-displacement and yaw accuracies for $dl_{max} = 10$ mm and $d\zeta_{f,max} = 0.2^\circ$	56

Bibliography

- [1] A. Pott, *Cable-driven parallel robots: theory and application*, vol. 120. Springer, 2018.
- [2] S.-R. Oh, J.-C. Ryu, and S. K. Agrawal, “Dynamics and Control of a Helicopter Carrying a Payload Using a Cable-Suspended Robot,” *Journal of Mechanical Design*, vol. 128, pp. 1113–1121, 12 2005.
- [3] A. Ming and T. Higuchi, “Study on multiple degree-of-freedom positioning mechanism using wires. concept, design and control,” *International Journal of The Japan Society for Precision Engineering*, vol. 28, pp. 131–138, 1994.
- [4] M. Carricato, “Direct Geometrico-Static Problem of Underconstrained Cable-Driven Parallel Robots With Three Cables,” *Journal of Mechanisms and Robotics*, vol. 5, 06 2013. 031008.
- [5] M. Carricato and G. Abbasnejad, “Direct geometrico-static analysis of underconstrained cable-driven parallel robots with 4 cables,” *Mechanisms and Machine Science*, vol. 12, pp. 269–285, 2013. cited By.
- [6] G. Abbasnejad and M. Carricato, “Direct geometrico-static problem of underconstrained cable-driven parallel robots with five cables,” in *Computational Kinematics* (F. Thomas and A. Perez Gracia, eds.), (Dordrecht), pp. 59–66, Springer Netherlands, 2014.
- [7] G. Abbasnejad and M. Carricato, “Direct geometrico-static problem of underconstrained cable-driven parallel robots with n cables,” *IEEE Transactions on Robotics*, vol. 31, pp. 468–478, April 2015.
- [8] V. Parenti-Castelli and R. Di Gregorio, “Real-Time Computation of the Actual Posture of the General Geometry 6-6 Fully-Parallel Mechanism Using Two Extra Rotary Sensors,” *Journal of Mechanical Design*, vol. 120, pp. 549–554, 12 1998.
- [9] I. Bonev, J. Ryu, S.-G. Kim, and S.-K. Lee, “A closed-form solution to the direct kinematics of nearly general parallel manipulators with optimally located three linear extra sensors,” *IEEE Transactions on Robotics and Automation*, vol. 17, no. 2, pp. 148–156, 2001.
- [10] J.-P. Merlet, “Direct kinematics of cdpr with extra cable orientation sensors: The 2 and 3 cables case with perfect measurement and ideal or elastic cables,” in *Cable-Driven Parallel Robots* (C. Gosselin, P. Cardou, T. Bruckmann, and A. Pott, eds.), (Cham), pp. 180–191, Springer, 2018.

- [11] J.-P. Merlet, "An experimental investigation of extra measurements for solving the direct kinematics of cable-driven parallel robots," in *2018 IEEE International Conference on Robotics and Automation (ICRA)*, pp. 6947–6952, 2018.
- [12] E. Idà, J.-P. Merlet, and M. Carricato, "Automatic self-calibration of suspended under-actuated cable-driven parallel robot using incremental measurements," in *Cable-Driven Parallel Robots* (A. Pott and T. Bruckmann, eds.), (Cham), pp. 333–344, Springer International Publishing, 2019.
- [13] A. Pott, "Influence of pulley kinematics on cable-driven parallel robots," in *Latest Advances in Robot Kinematics* (J. Lenarcic and M. Husty, eds.), pp. 197–204, Dordrecht: Springer, 2012.
- [14] E. Idà, T. Bruckmann, and M. Carricato, "Rest-to-rest trajectory planning for underactuated cable-driven parallel robots," *IEEE Transactions on Robotics*, vol. 35, pp. 1338–1351, Dec 2019.
- [15] A. Nubiola, M. Slamani, A. Joubair, and I. A. Bonev, "Comparison of two calibration methods for a small industrial robot based on an optical cmm and a laser tracker," *Robotica*, vol. 32, no. 3, p. 447–466, 2014.
- [16] D. Daney, N. Andreff, G. Chabert, and Y. Papegay, "Interval method for calibration of parallel robots: Vision-based experiments," *Mechanism and Machine Theory*, vol. 41, no. 8, pp. 929 – 944, 2006.
- [17] D. Lau, "Initial length and pose calibration for cable-driven parallel robots with relative length feedback," in *Cable-Driven Parallel Robots* (C. Gosselin, P. Cardou, T. Bruckmann, and A. Pott, eds.), (Cham), pp. 140–151, Springer International Publishing, 2018.
- [18] P. H. Borgstrom, B. L. Jordan, B. J. Borgstrom, M. J. Stealey, G. S. Sukhatme, M. A. Batalin, and W. J. Kaiser, "Nims-pl: A cable-driven robot with self-calibration capabilities," *IEEE Transactions on Robotics*, vol. 25, no. 5, pp. 1005–1015, 2009.
- [19] J.-P. Merlet, "Closed-form resolution of the direct kinematics of parallel manipulators using extra sensors data," vol. 1, pp. 200–204, 1993. cited By 108.
- [20] J. P. Merlet, "Jacobian, Manipulability, Condition Number, and Accuracy of Parallel Robots," *Journal of Mechanical Design*, vol. 128, pp. 199–206, 06 2005.
- [21] P. Cardou, S. Bouchard, and C. Gosselin, "Kinematic-sensitivity indices for dimensionally nonhomogeneous jacobian matrices," *IEEE Transactions on Robotics*, vol. 26, no. 1, pp. 166–173, 2010.
- [22] B. Mehrafrooz, M. Mohammadi, and M. T. Masouleh, "Kinematic sensitivity evaluation of revolute and prismatic 3-dof delta robots," in *2017 5th RSI International Conference on Robotics and Mechatronics (ICRoM)*, pp. 225–231, 2017.
- [23] V. Mattioni, E. Idà, and M. Carricato, "Force-distribution sensitivity to cable-tension errors: A preliminary investigation," in *Cable-Driven Parallel Robots* (M. Gouttefarde, T. Bruckmann, and A. Pott, eds.), (Cham), pp. 129–141, Springer International Publishing, 2021.

- [24] E. Idà and M. Carricato, “A new performance index for underactuated cable-driven parallel robots,” in *Cable-Driven Parallel Robots* (M. Gouttefarde, T. Bruckmann, and A. Pott, eds.), (Cham), pp. 24–36, Springer International Publishing, 2021.
- [25] G. Mottola, C. Gosselin, and M. Carricato, “Effect of actuation errors on a purely-translational spatial cable-driven parallel robot,” in *2019 IEEE 9th Annual International Conference on CYBER Technology in Automation, Control, and Intelligent Systems (CYBER)*, pp. 701–707, 2019.
- [26] J. M. Hendrickx and A. Olshevsky, “Matrix p -norms are np -hard to approximate if $p \neq 1, 2, \infty$,” *SIAM Journal on Matrix Analysis and Applications*, vol. 31, no. 5, pp. 2802–2812, 2010.
- [27] A. A. Kumar, J.-F. Antoine, P. Zattarin, and G. Abba, “Workspace analysis of a 4 cable-driven spatial parallel robot,” in *ROMANSY 22 – Robot Design, Dynamics and Control* (V. Arakelian and P. Wenger, eds.), (Cham), pp. 204–212, Springer International Publishing, 2019.
- [28] N. Johnston, “Quetlab: A matlab toolbox for quantum entanglement, version 0.9.” <http://qetlab.com>.